Article

Developmental Cell

Glutamine Metabolism Controls Chondrocyte Identity and Function

Graphical Abstract

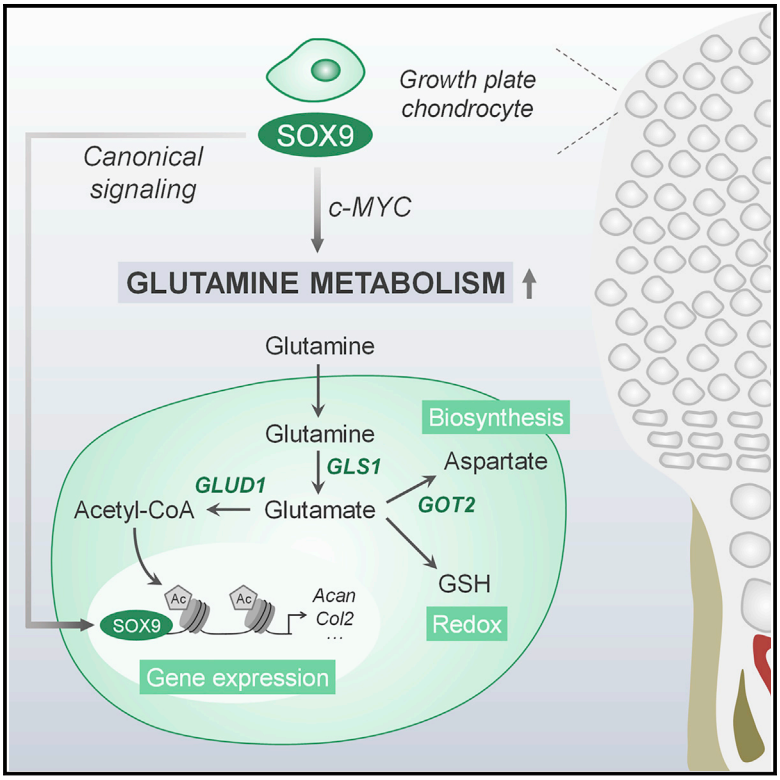

Authors

Steve Stegen, Gianmarco Rinaldi, Shauni Loopmans, ..., Sarah-Maria Fendt, Peter Carmeliet, Geert Carmeliet

Correspondence

geert.carmeliet@kuleuven.be

In Brief

Growth plate chondrocytes survive and function in an avascular environment, but their nutritional requirements are poorly characterized. Stegen et al. now demonstrate that the key chondrogenic transcription factor SOX9 induces glutamine metabolism, and this metabolic adaptation is in turn necessary to support chondrocyte gene expression, biosynthesis, and redox homeostasis.

Highlights

- The chondrogenic transcription factor SOX9 induces glutamine metabolism
- Glutamine-derived acetyl-CoA epigenetically regulates chondrogenic gene expression
- Transaminase-driven glutamine-derived aspartate controls chondrocyte biosynthesis
- Glutamine-dependent glutathione synthesis maintains chondrocyte redox homeostasis

Stegen et al., 2020, Developmental Cell *53*, 530–544
June 8, 2020
https://doi.org/10.1016/j.devcel.2020.05.001

CellPress

CellPress

Developmental Cell

Article

Glutamine Metabolism Controls Chondrocyte Identity and Function

Steve Stegen,[1] Gianmarco Rinaldi,[2,3] Shauni Loopmans,[1] Ingrid Stockmans,[1] Karen Moermans,[1] Bernard Thienpont,[4] Sarah-Maria Fendt,[2,3] Peter Carmeliet,[5,6,7] and Geert Carmeliet[1,8,*]

[1]Laboratory of Clinical and Experimental Endocrinology, Department of Chronic Diseases, Metabolism and Ageing, KU Leuven, Leuven, Belgium

[2]Laboratory of Cellular Metabolism and Metabolic Regulation, VIB Center for Cancer Biology, Leuven, Belgium

[3]Laboratory of Cellular Metabolism and Metabolic Regulation, Department of Oncology and Leuven Cancer Institute, KU Leuven, Leuven, Belgium

[4]Laboratory of Functional Epigenetics, Department of Human Genetics, KU Leuven, Leuven, Belgium

[5]Laboratory of Angiogenesis and Vascular Metabolism, VIB Center for Cancer Biology, Leuven, Belgium

[6]Laboratory of Angiogenesis and Vascular Metabolism, Department of Oncology and Leuven Cancer Institute, KU Leuven, Leuven, Belgium

[7]State Key Laboratory of Ophtalmology, Zhongshan Ophtalmic Center, Sun Yat-Sen University, Guangzhou, China

[8]Lead Contact

*Correspondence: geert.carmeliet@kuleuven.be

https://doi.org/10.1016/j.devcel.2020.05.001

SUMMARY

Correct functioning of chondrocytes is crucial for long bone growth and fracture repair. These cells are highly anabolic but survive and function in an avascular environment, implying specific metabolic requirements that are, however, poorly characterized. Here, we show that chondrocyte identity and function are closely linked with glutamine metabolism in a feedforward process. The master chondrogenic transcription factor SOX9 stimulates glutamine metabolism by increasing glutamine consumption and levels of glutaminase 1 (GLS1), a rate-controlling enzyme in this pathway. Consecutively, GLS1 action is critical for chondrocyte properties and function via a tripartite mechanism. First, glutamine controls chondrogenic gene expression epigenetically through glutamate dehydrogenase-dependent acetyl-CoA synthesis, necessary for histone acetylation. Second, transaminase-mediated aspartate synthesis supports chondrocyte proliferation and matrix synthesis. Third, glutamine-derived glutathione synthesis avoids harmful reactive oxygen species accumulation and allows chondrocyte survival in the avascular growth plate. Collectively, our study identifies glutamine as a metabolic regulator of cartilage fitness during bone development.

INTRODUCTION

Tissue growth highly depends on sufficient oxygen and nutrient supply to ensure that the mandatory biosynthetic and bioenergetic processes proceed optimally (Sullivan and Vander Heiden, 2019; Vander Heiden and DeBerardinis, 2017; Zhu and Thompson, 2019), and most tissues are therefore well vascularized. Long bone growth critically depends on the proper functioning of growth plate chondrocytes that, interestingly, reside and function in an environment devoid of blood vessels (Stegen and Carmeliet, 2019). Yet, chondrocytes are highly anabolic, as their proliferation and differentiation determine bone lengthening and the extracellular matrix they produce serves as a scaffold for osteoblast-mediated bone formation, which is crucial for normal endochondral ossification (Kronenberg, 2003; Long and Ornitz, 2013). This combination of high anabolism in an avascular milieu suggests that chondrocytes have a specific metabolic profile in order to fulfill their functions correctly.

However, little is known of how these cells metabolically operate in their specific microenvironment. Glucose is considered to be a crucial energy source and the main precursor for proteoglycan biosynthesis (Hollander and Zeng, 2019; Tchetina and Markova, 2018). Accordingly, chondrocyte-specific deletion of the key glucose transporter GLUT1 manifestly impairs chondrocyte proliferation and matrix synthesis, without affecting cell survival (Lee et al., 2018). Chondrocytes divert most of the glucose-derived carbons to the glycolytic pathway, which is energetically and biosynthetically less efficient compared with other metabolic pathways (Hollander and Zeng, 2019; Stegen et al., 2019; Tchetina and Markova, 2018). Yet, low levels of glucose oxidation are required to maintain an optimal energy status (Stegen et al., 2019). Thus, the fact that chondrocytes use the glycolytic pathway, together with their high biosynthetic needs, suggest that other nutrients complement glucose to fulfill these metabolic functions.

A potential nutrient that meets these requirements is glutamine, the most abundant amino acid in the circulation, which has a myriad of functions in cell metabolism. Studies in tumor cells show that glutamine can participate in ATP production, the generation of macromolecules and the antioxidant

glutathione, and may be involved in glycosaminoglycan synthesis (Altman et al., 2016; DeBerardinis and Cheng, 2010; Speight et al., 1978; Zhang et al., 2017). Critical in glutamine metabolism is the action of glutaminase (GLS), a rate-limiting enzyme that converts glutamine into glutamate, of which the GLS1 isoform is highly expressed in chondrocytes (Stegen et al., 2019). However, whether and how glutamine metabolism controls cartilage development and function is unknown. At the onset of cartilage formation, mesenchymal precursors differentiate to chondrocytes through the action of the master chondrogenic transcription factor sex determining region Y box 9 (SOX9) (Lefebvre et al., 2019). During this transition, these cells have to adapt to an avascular environment, but it is unclear whether SOX9 also controls this metabolic rewiring.

We therefore investigated the role of glutamine metabolism in growth plate chondrocytes during endochondral ossification. We show that SOX9 stimulates glutamine uptake and catabolism in chondrocytes. In turn, glutamine metabolism, through GLS1, coordinates chondrocyte gene expression, biosynthesis, and redox balance during bone development.

RESULTS

SOX9 Regulates Glutamine Metabolism in Chondrocytes

To explore whether chondrogenic lineage specification induced by SOX9 involves metabolic changes, we reanalyzed a SOX9-ChIP-seq (chromatin immunoprecipitation sequencing) dataset (Ohba et al., 2015) by ranking all putative SOX9 target genes according to SOX9 binding enrichment, followed by Gene Ontology analysis with focus on cell metabolism (Gaude and Frezza, 2016). Interestingly, glutamate metabolism (i.e., a proxy for glutamine metabolism) was highly ranked within the large group of metabolic pathways, just below pathways involved in nucleotide and extracellular matrix synthesis, and significantly higher than other metabolic pathways that are suggested to take part in the regulation of skeletal cell function, such as oxidative phosphorylation, tricarboxylic acid (TCA) cycle activity, glycolysis, gluconeogenesis, and fatty acid metabolism (Table S1). Together, these data suggest that SOX9 regulates metabolic pathways and stimulates glutamine metabolism in chondrocytes.

To verify that glutamine metabolism is stimulated in chondrocytes, we first analyzed glutamine uptake and catabolism compared with skeletal progenitors (Figure 1A). Lineage-committed growth plate chondrocytes (hereafter named chondrocytes) showed higher glutamine uptake, mRNA levels of a key glutamine transporter (*Slc1a5*) together with increased gene and protein expression of GLS1 compared with skeletal progenitors (Figures 1B, 1C, S1A, and S1B). In addition, using $^{13}C_5$-glutamine tracing, we observed higher ^{13}C-incorporation in intracellular glutamine in chondrocytes than in skeletal progenitors, which was subsequently more catabolized into metabolites involved in biosynthesis and redox homeostasis (Figures 1D and S1C).

We next explored whether the higher glutamine metabolism in chondrocytes was driven by SOX9. First, we observed that during the differentiation of skeletal progenitors to chondrocytes using a micromass culture system (Figure 1A), the mRNA levels of *Slc1a5* and *Gls1* increased progressively, concomitant with the increase in *Sox9* expression (Figures 1E, S1D, and S1E). Of note, mRNA levels of *Gls2*, which is expressed at relatively low levels in chondrocytes (Stegen et al., 2019), were not altered (Figure S1E). Second, we modulated SOX9 levels in high or low SOX9-expressing cells by knockdown or overexpression, respectively, and investigated the effect on glutamine metabolism. Overexpression of SOX9 in skeletal progenitors increased glutamine uptake, as well as GLS1 mRNA and protein levels, resulting in enhanced proliferation and matrix deposition without altering cell survival (Figures 1F, 1G, and S1F–S1K). In contrast, SOX9 deletion in chondrocytes had the opposite effect on glutamine-related metabolic parameters and impaired their function (Figures 1F, 1G, and S1F–S1K). Third, we analyzed SOX9 binding to several domains in the enhancer regions of *Gls1* and glutamine transporters, selected on the presence of a predicted SOX9-binding motif. ChIP-qPCR analysis revealed increased SOX9 binding to the enhancer region of the *Gls1* promoter in chondrocytes (Figure S1L), compared with skeletal progenitor cells that express SOX9 at low levels (Figure 1F) (van Gastel et al., 2020). However, we could not detect SOX9 binding to the enhancer region of glutamine transporters (Table S1), suggesting that the SOX9-dependent regulation of glutamine uptake is indirect. In tumor cells, the transcription factor c-MYC upregulates the expression of glutamine transporters and GLS1, resulting in a general reprogramming of glutamine metabolism (Stine et al., 2015). Since *c-Myc* is a putative SOX9 target gene (Ohba et al., 2015) and controls chondrocyte behavior (Zhou et al., 2011), we explored a possible role for c-MYC in the SOX9-dependent regulation of glutamine uptake and catabolism. We observed that c-MYC levels were higher in chondrocytes compared with skeletal progenitor cells, an effect that was driven directly by SOX9 transcriptional activation as evidenced by ChIP-qPCR (Figures 1H, S1M, and S1N). In addition, shRNA-mediated deletion of c-MYC in chondrocytes reduced not only glutamine uptake, but also GLS1 protein levels, resulting in a decrease in intracellular glutamine-derived metabolite levels (Figures 1I–1K, S1O, and S1P). Of note, *Gls1* mRNA levels remained constant in c-MYC-deficient chondrocytes (Figure S1Q), which is in line with the post-transcriptional regulation of GLS1 by c-MYC (Gao et al., 2009). Accordingly, c-MYC knockdown in SOX9-overexpressing skeletal progenitors blunted the increase in glutamine uptake and GLS1 protein expression, without altering *Gls1* mRNA levels, confirming important SOX9-mediated contribution of c-MYC (Figures 1L–1N, S1R, and S1S). Together, these data indicate that SOX9 activates glutamine metabolism at multiple levels in chondrocytes but predominantly through induction of c-MYC (Figure S1T).

Deletion of GLS1 in Chondrocytes Affects Longitudinal Bone Growth

To determine whether glutamine metabolism has a physiological role during endochondral bone formation, we deleted GLS1 in growth plate chondrocytes, by crossing $Gls1^{lox/lox}$ mice with *type 2 collagen* (*Col2*)-Cre transgenic mice ($Gls1^{chon-}$), resulting in specific and efficient deletion of GLS1 at the mRNA and protein level (Figures 2A, S2A, and S2B). $Gls1^{chon-}$ mice were viable and indistinguishable from wild-type littermates at birth, but they displayed progressively stunted growth, evidenced by

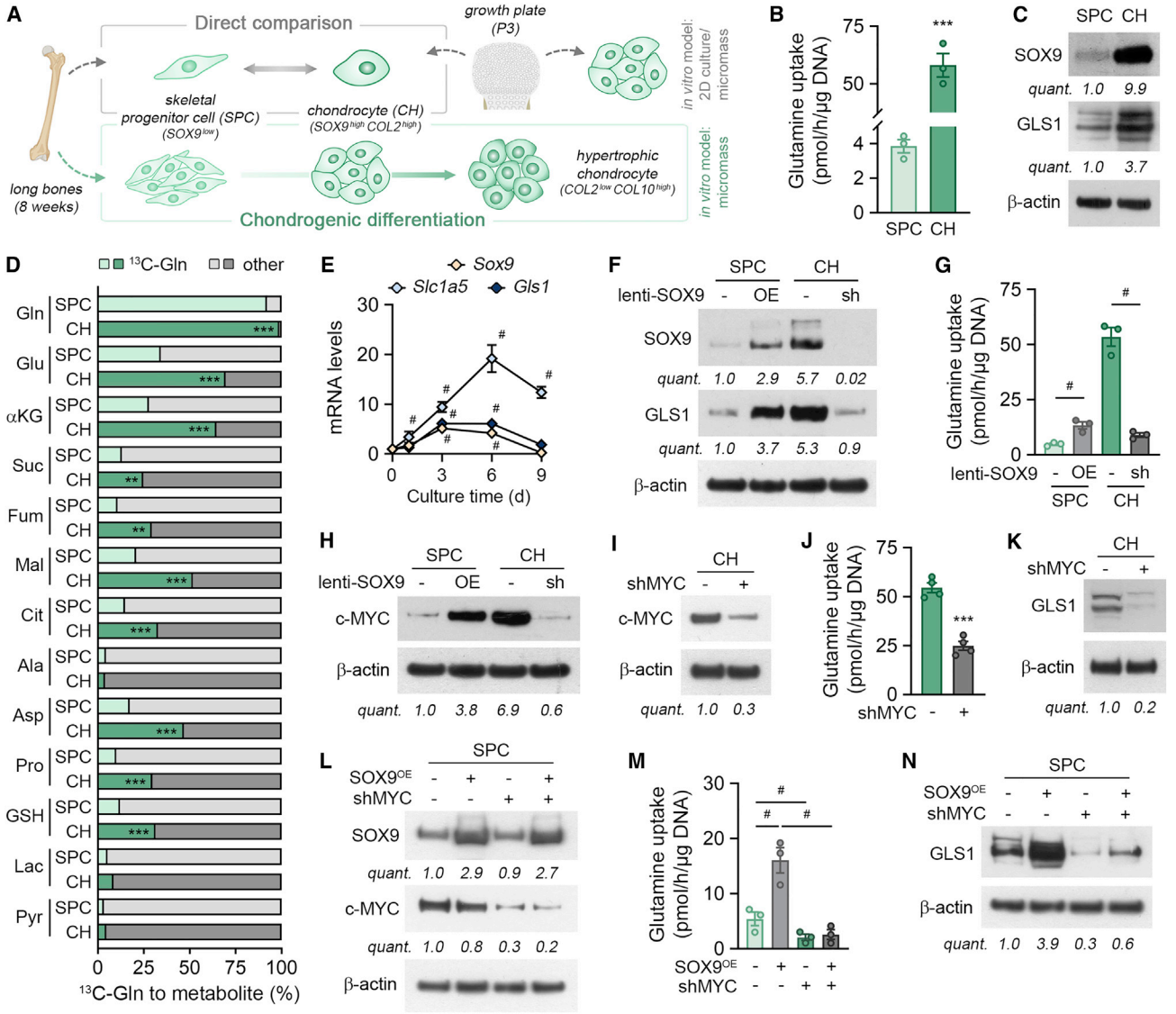

Figure 1. SOX9 Links Glutamine Metabolism to Chondrogenesis

(A) Schematic representation of experimental setup. Skeletal progenitor cells (SPCs) were isolated from long bones and either directly compared with lineage-committed chondrocytes (CHs) isolated from post-natal day 3 (P3) growth plates (gray path) or cultured as micromasses in chondrogenic medium for 9 days (green path). For other experiments, CHs were cultured as micromasses in growth medium unless otherwise specified.

(B) Glutamine uptake in SPCs and CHs (n = 3).

(C) Immunoblot of SOX9, GLS1, and β-actin levels in cultured SPCs and CHs (n=3).

(D) Fractional contribution of $^{13}C_5$-glutamine (Gln) to intracellular Gln, glutamate (Glu), α-ketoglutarate (αKG), succinate (Suc), fumarate (Fum), malate (Mal), citrate (Cit), alanine (Ala), aspartate (Asp), proline (Pro), reduced glutathione (GSH), lactate (Lac), and pyruvate (Pyr) in cultured SPCs and CHs (n = 4).

(E) *Sox9*, *Slc1a5*, and *Gls1* mRNA levels in micromass cultures (n = 3).

(F) Immunoblot of SOX9, GLS1, and β-actin levels in SPCs and CHs after transduction with a lentiviral vector carrying a SOX9-overexpression (OE) plasmid or a shRNA (sh) against SOX9, respectively (n = 3). An empty vector or scrambled shRNA were used as respective controls.

(G) Glutamine uptake in SPCs and CHs after transduction with a lentiviral vector carrying a SOX9-OE plasmid or a shRNA against SOX9 (n = 3).

(H) Immunoblot of c-MYC and β-actin levels in SPCs and CHs after transduction with a lentiviral vector carrying a SOX9-OE plasmid or a shRNA against SOX9 (n = 3).

(I) Immunoblot of c-MYC and β-actin levels in chondrocytes after transduction with a lentiviral vector carrying a shRNA against c-MYC (n = 3). A scrambled shRNA was used as control.

(J and K) Glutamine uptake (J) and immunoblot of GLS1 and β-actin levels (K) in chondrocytes after shRNA-mediated c-MYC knockdown (n = 4).

(L) Immunoblot of SOX9, c-MYC, and β-actin levels in SOX9-overexpressing skeletal progenitors after shRNA-mediated c-MYC knockdown (n = 3).

(M and N) Glutamine uptake (M) and immunoblot of GLS1 and β-actin levels (N) in SOX9-overexpressing skeletal progenitors after shRNA-mediated c-MYC knockdown (n = 3).

Data are means ± SEM. $^{\#}p < 0.05$ (ANOVA), $^{***}p < 0.001$ versus SPC-scrambled (scr) shRNA (Student's t-test). See also Figure S1; Table S1.

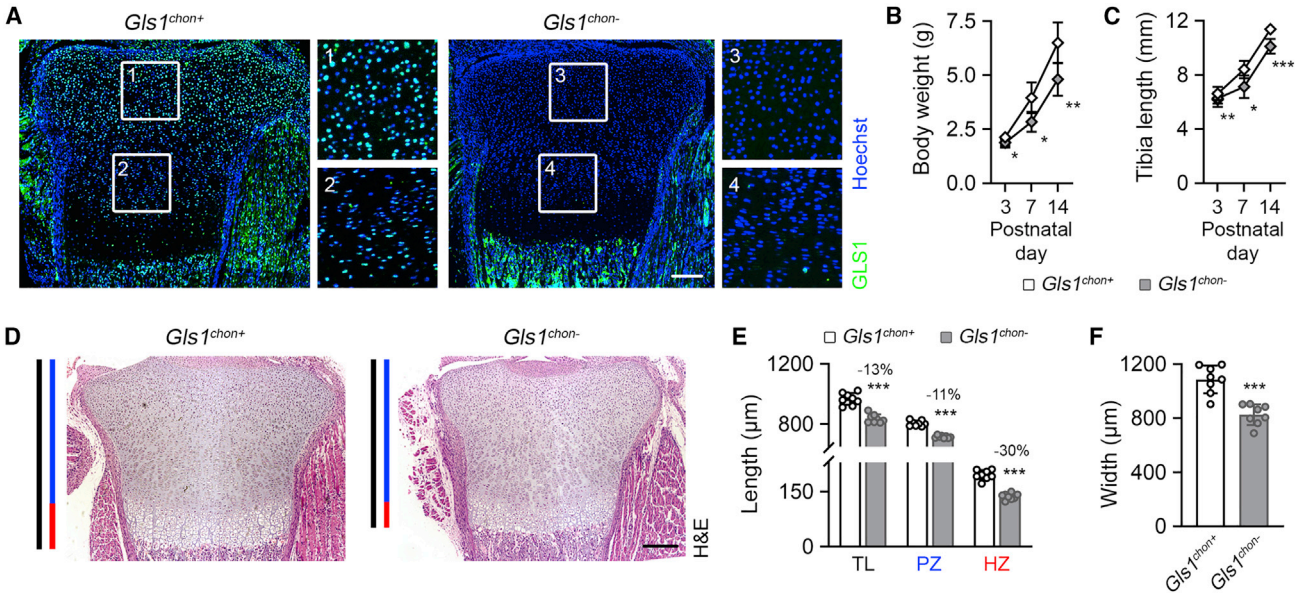

Figure 2. GLS1 in Chondrocytes Controls Bone Growth

(A) GLS1 immunostaining of neonatal growth plates from wild-type (*Gls1*$^{chon+}$) and chondrocyte-specific GLS1 knockout (*Gls1*$^{chon-}$) mice (n = 8). Boxed areas are magnified.

(B and C) Body weight (B) and tibia length (C) of mice at postnatal day 3 (P3), P7, and P14 (n = 8).

(D–F) H&E staining of the growth plate of tibia at P3 (D), with quantification (E) of the total length (TL), length of the proliferating (PZ) and hypertrophic zone (HZ), and width (F) of the growth plate (n = 8).

Data are means ± SD, scale bars in (A) and (D) are 200 μm. *p < 0.05 versus *Gls1*$^{chon+}$, **p < 0.01 versus *Gls1*$^{chon+}$, ***p < 0.001 versus *Gls1*$^{chon+}$ (Student's t-test). See also Figure S2.

decreased body weight and bone length (Figures 2B, 2C, and S2C). The decrease in size was not caused by changes in lean mass, fat mass, or serum metabolite levels (Figures S2D–S2F) but likely resulted from a cartilage-specific phenotype. Indeed, histomorphometric analysis of *Gls1*$^{chon-}$ tibiae revealed that already 3 days after birth, growth plate size was significantly decreased, with a reduction in growth plate length and width (Figures 2D–2F). Taken together, glutamine metabolism, through GLS1, regulates chondrocyte behavior during endochondral bone formation.

Glutamine Metabolism Regulates Chondrocytic Gene Expression through Histone Acetylation

The global reduction in growth plate size suggested impaired chondrocyte function. We found that deletion of GLS1 significantly decreased chondrogenic marker gene expression in the growth plate, without affecting *Sox9* mRNA levels (Figure 3A). Accordingly, using an *in vitro* micromass model starting from growth plate chondrocytes (Figure 1A), we found that the expression of early and late chondrocyte marker genes was also significantly decreased upon pharmacological GLS1 inactivation with bis-2-(5-phenylacetamido-1,2,4-thiadiazol-2-yl)ethyl sulfide (BPTES) or when chondrocyte micromasses were cultured in decreasing glutamine concentrations (Figure 3A). Thus, the master chondrogenic transcription factor SOX9 induces glutamine metabolism, which in turn is necessary to obtain adequate chondrocyte gene expression.

A possible explanation for reduced gene expression when cell metabolism is changed is epigenetic modification, as several intermediates of the TCA cycle are used as metabolic co-substrates or inhibitors for histone and DNA-modifying enzymes (Kinnaird et al., 2016; Reid et al., 2017). As a co-substrate, α-ketoglutarate (αKG) stimulates enzymatic activity of DNA and histone demethylases (Kinnaird et al., 2016; Reid et al., 2017), whereas enzyme activity is inhibited by succinate, fumarate, and 2-hydroxyglutarate (2HG). In cultured chondrocytes, $^{13}C_5$-glutamine tracing revealed that glutamine donated carbons to several of these TCA cycle intermediates, often even more than $^{13}C_6$-glucose, and accordingly, inhibition of GLS1 depleted intracellular αKG, succinate, fumarate, and malate pools (Figures 3B, 3C, S3A, and S3B). However, the levels of these metabolites were decreased to the same extent after GLS1 inhibition resulting in unaltered αKG/succinate, αKG/fumarate, and αKG/2HG ratios (Figure S3C). Accordingly, we could not detect changes in DNA hydroxymethylation, as evidenced by 5hmC dot blot, or in histone 3 (H3) methylation (Figures S3D and S3E).

In addition to DNA and histone methylation, chondrogenic gene expression is also regulated by changes in histone acetylation (Furumatsu and Asahara, 2010). We found that glutamine metabolism controls chondrocyte gene expression via histone acetylation, based on the following observations. First, GLS1 inactivation in chondrocytes reduced histone acetylation. More specifically, acetylation of histone 2A lysine 5 (H2AK5Ac) and H3K (H3KAc) were decreased in BPTES-treated cells, whereas H4K8Ac levels were not altered (Figures 3D, 3E, and S3F–S3H). Further analysis was focused on H3K9Ac and H3K27Ac, since these are considered as key epigenetic marks for active chondrogenic gene promotors (Herlofsen et al., 2013). In line

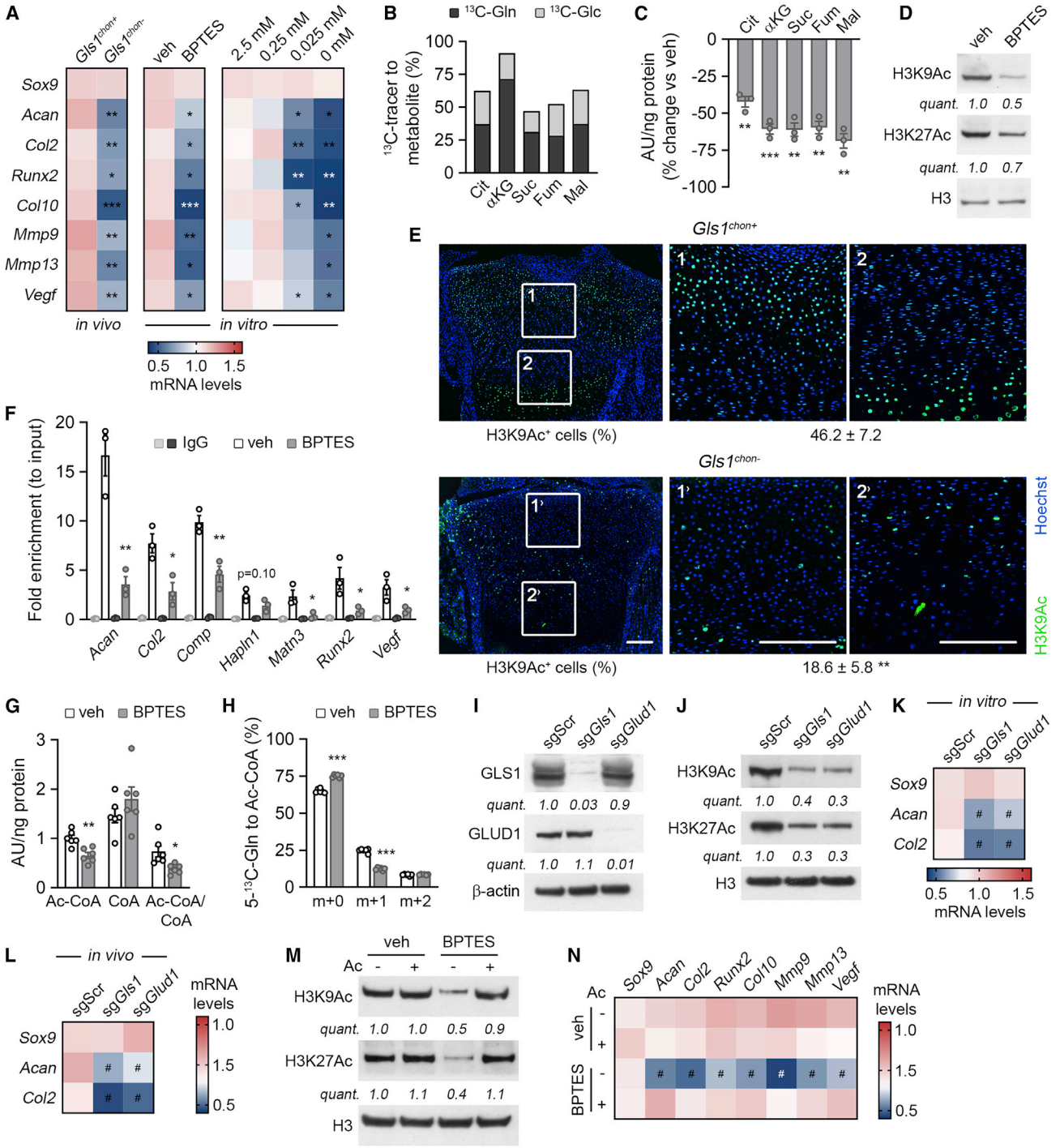

Figure 3. GLS1 Is Necessary for Chondrogenic Gene Expression and Histone Acetylation

(A) *Sox9*, *Acan*, *Col2*, *Runx2*, *Col10*, *Mmp9*, *Mmp13*, and *Vegf* mRNA levels in growth plates from neonatal wild type (*Gls1*$^{chon+}$) and chondrocyte-specific GLS1-deficient (*Gls1*$^{chon-}$) mice (left panel; n = 8), or in chondrocytes after vehicle (veh) or BPTES treatment (middle panel; n = 3) or after culture in decreasing glutamine concentrations (right panel; n = 3).

(B) Fractional contribution of $^{13}C_5$-Gln and $^{13}C_6$-glucose (Glc) to Cit, αKG, Suc, Fum, and Mal in cultured chondrocytes (n = 6).

(C) Intracellular Cit, αKG, Suc, Fum, and Mal levels in BPTES-treated chondrocytes as percent change versus veh-treated cells (n = 3).

(D) Immunoblot of acetylated H3 at lysine 9 (H3K9Ac), H3K27Ac, and total H3 (H3) levels in veh or BPTES-treated chondrocytes (n = 3).

(E) H3K9Ac immunostaining of neonatal growth plates, with quantification of the percentage H3K9Ac-positive cells (n = 8). Boxed areas are magnified, scale bar is 200 μm.

(legend continued on next page)

with the BPTES-induced changes in histone acetylation, glutamine deprivation of cultured chondrocytes elicited a dose-dependent decrease in H3K9Ac and H3K27Ac levels (Figure S3I). Second, we performed H3K27Ac ChIP-qPCR analysis to mechanistically link the changes in histone acetylation upon GLS1 inactivation with decreased chondrocyte gene expression. From a previously deposited H3K27Ac ChIP-seq dataset (Ohba et al., 2015), we selected chondrocyte-related genes (*Aggrecan* [*Acan*], *Col2*, *Cartilage oligomeric matrix protein*, *Hyaluronan and proteoglycan link protein 1*, *Matrilin-3*, *Runt-related transcription factor 2*, and *Vascular endothelial growth factor*) and genes involved in general cellular processes (*Cyclin D1* for proliferation, *Nedd4 Family Interacting Protein 2*, and *WW domain-containing protein 2* for protein processing, *Xylosyltransferase 1* for extracellular matrix synthesis). Interestingly, GLS1 inhibition only decreased the acetylation status of the chondrogenesis-related genes but not of the ones that control more general cellular processes (Figures 3F and S3J). These GLS1-dependent effects in histone acetylation were also reflected at the gene expression level (Figures 3A, S3K, and S3L), indicating that the decrease in chondrogenic marker gene expression observed in BPTES-treated cells is directly linked to reduced H3K acetylation. Finally, GLS1 inhibition blocked the increase in H3K9Ac and H3K27Ac levels and chondrogenic gene expression induced by the histone deacetylase inhibitor trichostatin A (Figures S3M and S3N).

Together, these findings suggest that glutamine-derived metabolites serve as metabolic substrates for H3K acetylation. Indeed, histone acetylation is highly sensitive to the availability of acetyl-coenzyme A (CoA) (Sivanand et al., 2018) and GLS1 inhibition in chondrocytes reduced acetyl-CoA levels without affecting CoA, resulting in a decreased acetyl-CoA/CoA ratio (Figure 3G). In mammals, the production of acetyl-CoA from glutamine occurs in a step-wise process. First, glutamine generates citrate via reductive carboxylation or glutamine oxidation, and the conversion of glutamate into αKG by glutamate dehydrogenase 1 (GLUD1) is an important first step herein (Altman et al., 2016; DeBerardinis and Cheng, 2010). Subsequently, citrate is transported to the nucleus, where it is converted to acetyl-CoA by ATP-citrate lyase, which provides a local acetyl pool for histone acetylation (Kinnaird et al., 2016; Sivanand et al., 2018). In chondrocytes, 5-^{13}C-glutamine tracing experiments showed that glutamine-derived carbons were labeling a substantial proportion of the acetyl-CoA pool via reductive carboxylation, which was decreased upon inhibition of GLS1 (Figures 3H, S3O, and S3P). In line, deletion of GLUD1 in cultured chondrocytes mimicked the reduction in H3K acetylation, and *Acan* and *Col2* mRNA expression observed in GLS1-deficient cells (Figures 3I–3K). These *in vitro* findings were confirmed *in vivo* using an ectopic model of endochondral bone formation (Stegen et al., 2019; van Gastel et al., 2014), where we implanted chondrogenically primed cells subcutaneously in mice: GLS1 or GLUD1 deletion impaired chondrogenic gene expression (Figures 3L and S3Q).

To further prove the epigenetic effects mediated by glutamine metabolism, we reasoned that supplementation with acetate, which can be converted into acetyl-CoA by acetyl-CoA synthetase (Kinnaird et al., 2016; Sivanand et al., 2018), could replenish the acetyl-CoA pools and recover the gene expression defect caused by GLS1 inhibition. Acetate addition to BPTES-treated cells restored H3K9Ac and H3K27Ac levels and the expression of chondrogenic markers (Figures 3M and 3N). Together, these results demonstrate that in chondrocytes, H3K acetylation and chondrogenic marker gene expression are dependent on glutamine metabolism through a GLS1-GLUD1 axis.

Glutamine Supports Chondrocytic Biosynthesis

Chondrocyte-specific gene expression is only one aspect of normal endochondral bone formation, and maintaining biosynthetic processes, such as proliferation and matrix synthesis are equally important (Kronenberg, 2003). The decrease in growth plate length in *Gls1*$^{chon-}$ mice suggested reduced chondrocyte proliferation, which was evidenced by reduced Ki67 immunostaining in *Gls1*$^{chon-}$ growth plates and further confirmed *in vitro* during glutamine deprivation or after BPTES treatment (Figures 4A–4C). Along with the decrease in proliferation, glutamine deprivation or GLS1 inhibition impaired global protein synthesis as well as collagen and matrix production in chondrocytes *in vitro*, effects that mirrored the reduction in COL2 immunostaining in mutant growth plates (Figures 4D–4I).

A possible explanation of this biosynthetic defect could be a decrease in gene expression caused by epigenetic alterations. However, acetate supplementation did not rescue the decrease in proliferation and protein synthesis induced by GLS1 inhibition in cultured chondrocytes (Figures S3R and S3S). To further dissect the underlying mechanism, we first focused on energy homeostasis, as it is known that other (malignant) cell types rely on glutamine oxidation for generating ATP (Altman et al., 2016; DeBerardinis and Cheng, 2010; Zhang et al., 2017). In chondrocytes, however, glutamine metabolism was dispensable for energy homeostasis, as inhibition of GLS1 did not alter intracellular ATP

(F) ChIP-qPCR analysis of H3K27Ac enrichment in the enhancer region of *Acan*, *Col2*, *Comp*, *Hapln1*, *Matn3*, *Runx2*, and *Vegf* in veh and BPTES-treated chondrocytes (n = 3). Species-specific immunoglobulin G (IgG) antibodies were used as control.
(G) Quantification of acetyl-CoA (Ac-CoA) species in veh and BPTES-treated chondrocytes (n = 6).
(H) Acetyl-CoA labeling from 5-^{13}C-Gln (n = 6). M+1 indicates specific carbon labeling from glutamine via reductive carboxylation.
(I and J) Immunoblot of GLS1, GLUD1 (I), H3K9Ac, H3K27Ac (J), β-actin, and H3 levels in chondrocytes, transduced with a lentiviral vector containing Cas9 and Scr or gene-specific sgRNA (n = 3).
(K) *Sox9*, *Acan*, and *Col2* mRNA levels in chondrocytes, transduced with a lentiviral vector containing Cas9 and sgScr or gene-specific sgRNA (n = 3).
(L) *Sox9*, *Acan*, and *Col2* mRNA levels in ectopic implants (n = 5). GLS1 and GLUD1 were deleted from chondrogenically primed skeletal progenitors as described in (I) prior to ectopic implantation.
(M) Immunoblot of H3K9Ac, H3K27Ac, and H3 levels in veh and BPTES-treated chondrocytes, with or without acetate supplementation (n = 3).
(N) *Sox9*, *Acan*, *Col2*, *Runx2*, *Col10*, *Mmp9*, *Mmp13*, and *Vegf* mRNA levels in veh and BPTES-treated chondrocytes, with or without acetate (Ac) supplementation (n = 3).
Data are means ± SD (A-left panel and E) or means ± SEM (A-middle and right panel, B, C, F, G, and H). *p < 0.05 versus *Gls1*$^{chon+}$ or veh or 2.5 mM, **p < 0.01 versus *Gls1*$^{chon+}$ or veh or 2.5 mM, ***p < 0.001 versus *Gls1*$^{chon+}$ or veh or 2.5 mM (Student's t-test), $^{\#}$p < 0.05 (ANOVA). See also Figure S3.

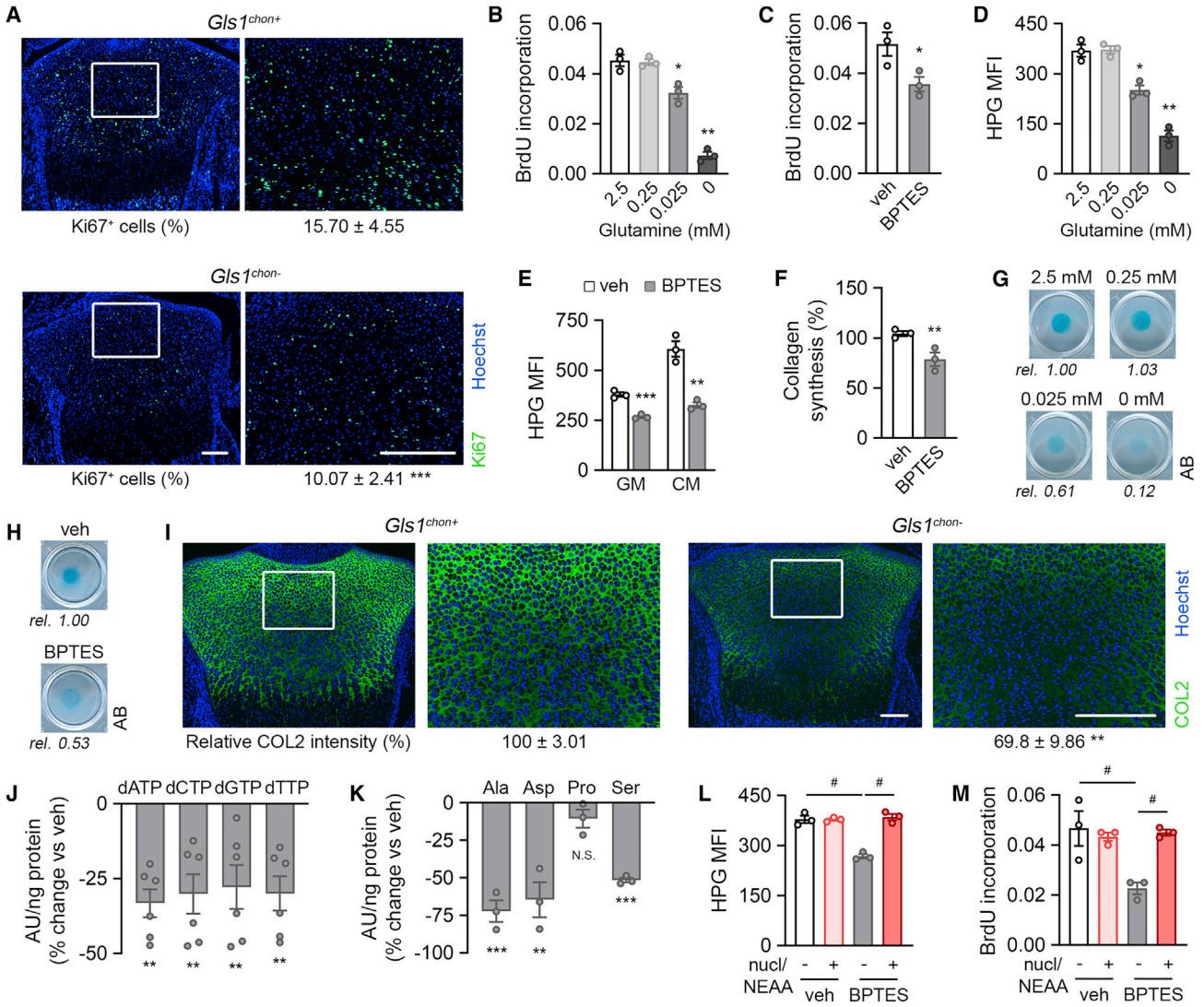

Figure 4. GLS1 Controls Chondrocyte Biosynthesis

(A) Ki67 immunostaining of neonatal growth plates, with quantification of the percentage Ki67-positive cells (n = 8). Boxed areas are magnified.

(B and C) Proliferation, as determined by BrdU incorporation, of chondrocytes cultured in decreasing glutamine concentrations (B) or during BPTES treatment (C) (n = 3).

(D and E) Protein synthesis, as determined by L-homopropargylglycine (HPG) mean fluorescence intensity (MFI), in chondrocytes cultured in decreasing glutamine concentrations (D) or after BPTES addition to normal growth medium (GM) or chondrogenic medium (CM) (E) (n = 3).

(F) Collagen synthesis in veh or BPTES-treated chondrocytes (n = 3).

(G and H) Chondrogenic matrix deposition by chondrocytes cultured as micromasses in decreasing glutamine concentrations (G) or in the presence of BPTES (H), as determined by alcian blue (AB) staining (n = 3).

(I) Type 2 collagen (COL2) immunostaining of neonatal growth plates, with quantification of the relative COL2 signal intensity (n = 8). Boxed areas are magnified.

(J) Intracellular dNTP levels in BPTES-treated chondrocytes as percent change versus veh-treated cells (n = 6).

(K) Intracellular Ala, Asp, Pro, and serine (Ser) levels in BPTES-treated chondrocytes as percent change versus veh-treated cells (n=3).

(L) Protein synthesis by veh and BPTES-treated chondrocytes, with or without nucleotides (nucl) and NEAA supplementation (n = 3).

(M) Proliferation, as determined by BrdU incorporation, of veh and BPTES-treated chondrocytes, with or without nucl and NEAA supplementation (n = 3).

Data are means ± SD (A and I) or means ± SEM (B–F and J–M). *$p < 0.05$ versus 2.5 mM or veh or *Gls1*$^{chon+}$, **$p < 0.01$ versus 2.5 mM or veh or *Gls1*$^{chon+}$, ***$p < 0.001$ versus 2.5 mM or veh or *Gls1*$^{chon+}$ (Student's t-test), $^{\#}p < 0.05$ (ANOVA), N.S. is not significant. Scale bars in (A) and (I) are 200 μm. See also Figure S4.

levels, energy charge (defined as [ATP] + 1/2 [ADP]/[ATP] + [ADP] + [AMP]) or ADP/ATP ratio (Figures S4A–S4C). Consequently, we could not detect activation of AMPK signaling (Figure S4D), further confirming that the biosynthesis defect in BPTES-treated cells was not caused by an energy deficit.

Glutamine can also serve as a metabolic precursor for the production of macromolecules, such as nucleotides and amino acids, in order to support proliferation and protein synthesis (Altman et al., 2016; DeBerardinis and Cheng, 2010; Lane and Fan, 2015; Vander Heiden and DeBerardinis, 2017). Consistent with

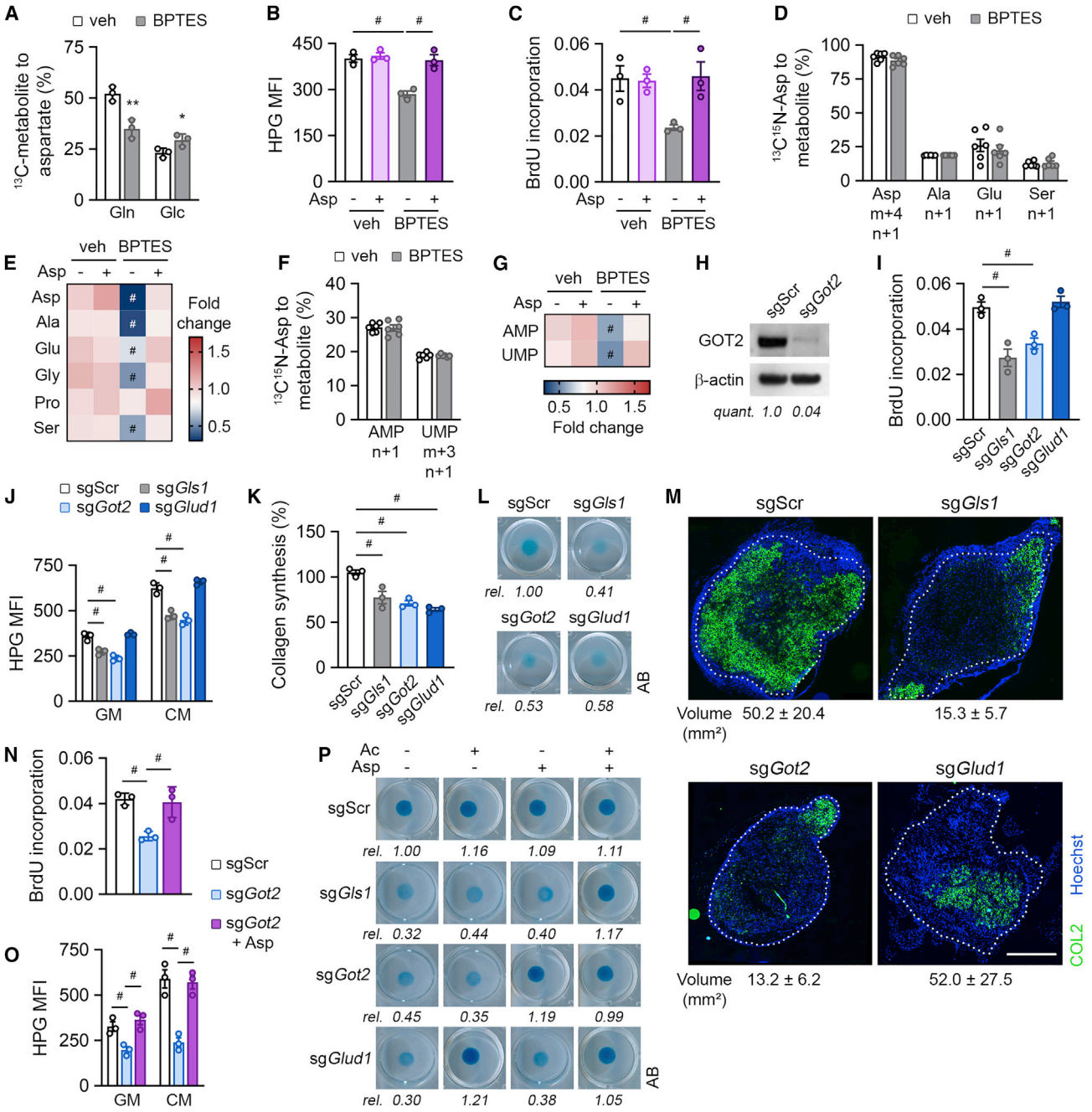

Figure 5. Chondrocyte Biosynthesis Is Regulated by a GLS1-GOT2 Pathway

(A) Fractional contribution of $^{13}C_5$-Gln and $^{13}C_6$-Glc to Asp in veh and BPTES-treated chondrocytes (n = 3).

(B) Protein synthesis, as determined by determined by L-homopropargylglycine (HPG) MFI, by veh and BPTES-treated chondrocytes, with or without Asp supplementation (n = 3).

(C) Proliferation, as determined by BrdU incorporation, of veh and BPTES-treated chondrocytes, with or without Asp supplementation (n = 3).

(D) Isotopic labeling of Asp, Ala, Glu, and Ser from $^{13}C_4{}^{15}N$-Asp (n = 6). Specific mass distribution vectors for each metabolite are shown; m and n are carbon and nitrogen label, respectively.

(E) Intracellular Asp, Ala, Glu, glycine (Gly), Pro, and Ser levels in veh and BPTES-treated chondrocytes with or without aspartate supplementation (n = 6).

(F) Isotopic labeling of purines (AMP) and pyrimidines (UMP) from $^{13}C_4{}^{15}N$-Asp (n = 6). Specific mass distribution vectors for each metabolite are shown; m and n are carbon and nitrogen label, respectively.

(G) Intracellular AMP and UMP levels in veh and BPTES-treated chondrocytes with or without aspartate supplementation (n = 6).

(H) Immunoblot of GOT2 and β-actin levels in chondrocytes, transduced with a lentiviral vector containing Cas9 and Scr or *Got2*-specific sgRNA (n = 3).

(I–K) Proliferation (I), protein synthesis (J), and collagen synthesis (K) of GLS1, GOT2, and GLUD1-deficient chondrocytes (n = 3).

(L) Chondrogenic matrix deposition by GLS1, GOT2, and GLUD1-deficient chondrocytes, as determined by AB staining of micromasses (n = 3).

(legend continued on next page)

the proliferation defect, we observed a significant decrease in purine (dATP and dGTP) and pyrimidine (dCTP and dTTP) deoxyribonucleotide levels, which was associated with G_0/G_1 cell-cycle arrest (Figures 4J and S4E). Moreover, several glutamine-derived non-essential amino acids (NEAAs), including alanine, aspartate, and serine, were decreased in BPTES-treated chondrocytes (Figure 4K), which can explain the reduced protein synthesis. To substantiate the link between inhibition of GLS1, decreased nucleotide and NEAA levels, and proliferation, we supplemented chondrocytes with a nucleoside mixture and/or NEAAs. Whereas nucleosides or NEAAs alone did not affect proliferation (Figure S4F), combined administration prevented cell-cycle arrest and restored protein synthesis in BPTES-treated chondrocytes, thereby fully rescuing the proliferation defect (Figures 4L, 4M, and S4G).

Chondrocytes Depend on Glutamine for Aspartate Synthesis via Mitochondrial Aspartate Transaminase

To further understand how glutamine contributes to biosynthesis in chondrocytes, we investigated which glutamine-derived metabolites are crucial for macromolecule generation. Aspartate is a plausible candidate, as it serves as a precursor of nucleotides and is involved in protein synthesis (Altman et al., 2016; Vander Heiden and DeBerardinis, 2017). $^{13}C_5$-glutamine tracing experiments revealed a high contribution (~50%) of glutamine-derived carbons to aspartate, which was decreased in BPTES-treated cells (Figure 5A). Chondrocytes responded to GLS1 inhibition by increasing aspartate uptake, resulting in medium depletion, and by enhancing carbon flux from glucose (Figures 5A, S4H, and S4I), but these adaptations were insufficient to maintain intracellular aspartate levels (Figure 4K), suggesting that chondrocytes critically depend on glutamine for *de novo* aspartate synthesis. To confirm this hypothesis, we supplied BPTES-treated cells with aspartate at a supra-physiological concentration, which resulted in a complete rescue of the cell-cycle defect, the decrease in protein synthesis and the reduced proliferation (Figures 5B, 5C, and S4J). Mechanistically, aspartate-derived carbon and nitrogen was incorporated in amino acids and nucleotides, thereby normalizing their levels in BPTES-treated cells (Figures 5D–5G and S4K). This metabolic rescue was, however, not sufficient to fully restore matrix deposition by BPTES-treated chondrocytes, likely because of the persisting decrease in *Acan* and *Col2* gene expression (Figures S4L and S4M). Indeed, aspartate-dependent acetyl-CoA labeling via TCA cycle anaplerosis was only minimal and, consequently, aspartate supplementation did not restore the acetyl-CoA levels needed for histone acetylation and gene expression (Figures S4N and S4O). Accordingly, co-supplementation of acetate and aspartate fully rescued the defects in gene expression and matrix deposition to the level of vehicle-treated cells (Figures S4L and S4M).

Next, we investigated the pathway by which glutamine is converted into aspartate. In theory, uniformly ^{13}C-labeled aspartate can be derived from glutamine either following (1) the canonical GLUD1-mediated conversion of glutamate to αKG or (2) the non-canonical mitochondrial aspartate transaminase (GOT2)-mediated conversion of oxaloacetate and glutamate to aspartate and αKG (Altman et al., 2016). To discriminate between these two pathways, we treated chondrocytes with either epigallocatechin gallate (EGCG), an inhibitor of GLUD1, or aminooxyacetate (AOA), a pan-inhibitor of transaminases (TAs). Whereas EGCG had no effect, AOA treatment inhibited chondrocyte growth and proliferation (Figures S5A–S5C), suggesting that transaminases, rather than GLUD1, control chondrocyte biosynthesis. In line, administration of AOA, but not EGCG, to wild-type mice resulted in decreased bone length (Figure S5D), indicative of a biosynthetic defect (Baron et al., 2015). To confirm these results, we genetically targeted GLUD1 and GOT2 using CRISPR-Cas9 (Figures 3I and 5H). GOT2 knockdown negatively affected chondrocyte biosynthesis including growth, proliferation, and protein and collagen synthesis *in vitro* and *in vivo*, whereas GLUD1 deletion only decreased collagen synthesis (Figures 5I–5M, S5E, and S5F). Consistent with these observations and the fact that glutamine is necessary for aspartate generation, GLUD1 knockdown did not affect aspartate levels, whereas GOT2 knockdown resulted in a significant decrease, similar as observed in GLS1-deficient cells (Figure S5G). In accordance, rescue with aspartate fully restored the proliferation rate and protein and matrix synthesis of GOT2-deficient cells (Figures 5N–5P). Importantly, concerning collagen synthesis, both GOT2 and GLUD1 are required (Figures 5K and 5L) but through different mechanisms. GLUD1 deletion impaired collagen synthesis by decreasing *Col2* gene expression by epigenetic mechanisms and supplementation with acetate fully restored matrix deposition by GLUD1-deficient cells (Figures 3N, 3O, and 5P). In contrast, silencing GOT2 did not affect histone acetylation nor chondrogenic gene expression (Figures S5H and S5I) but decreased biosynthetic pathways, indicating that chondrocytes allocate glutamine-derived carbons for specific metabolic functions via different pathways. Taken together, these data demonstrate that chondrocytes metabolize glutamine to maintain macromolecule synthesis via GOT2-dependent *de novo* aspartate synthesis.

GLS1 Regulates Chondrocyte Viability by Maintaining Redox Homeostasis

Glutamine is thus an important nutrient for chondrocyte biosynthesis. However, restoring biomass production did not fully rescue the number of BPTES-treated cells (Figure 6A), suggesting that glutamine metabolism controls additional cellular

(M) Type 2 collagen (COL2) immunostaining of ectopic implants, with quantification of implant volume upon deletion of GLS1, GOT2, or GLUD1 (n = 4–5). Scale bar is 500 μm.
(N–O) Proliferation (N) and protein synthesis (O) of GOT2-deficient chondrocytes, with or without Asp supplementation (n = 3).
(P) Chondrogenic matrix deposition by GLS1, GOT2, or GLUD1-deficient chondrocytes, with or without Ac or Asp supplementation, as determined by AB staining of micromasses (n = 3).
In (J) and (O), GM is growth medium and CM is chondrogenic medium.
Data are means ± SEM (A–D, F, H–K, N, and O) or means ± SD (M). *$p < 0.05$ versus veh, **$p < 0.01$ versus veh (Student's t-test), $^{\#}p < 0.05$ (ANOVA). See also Figure S5.

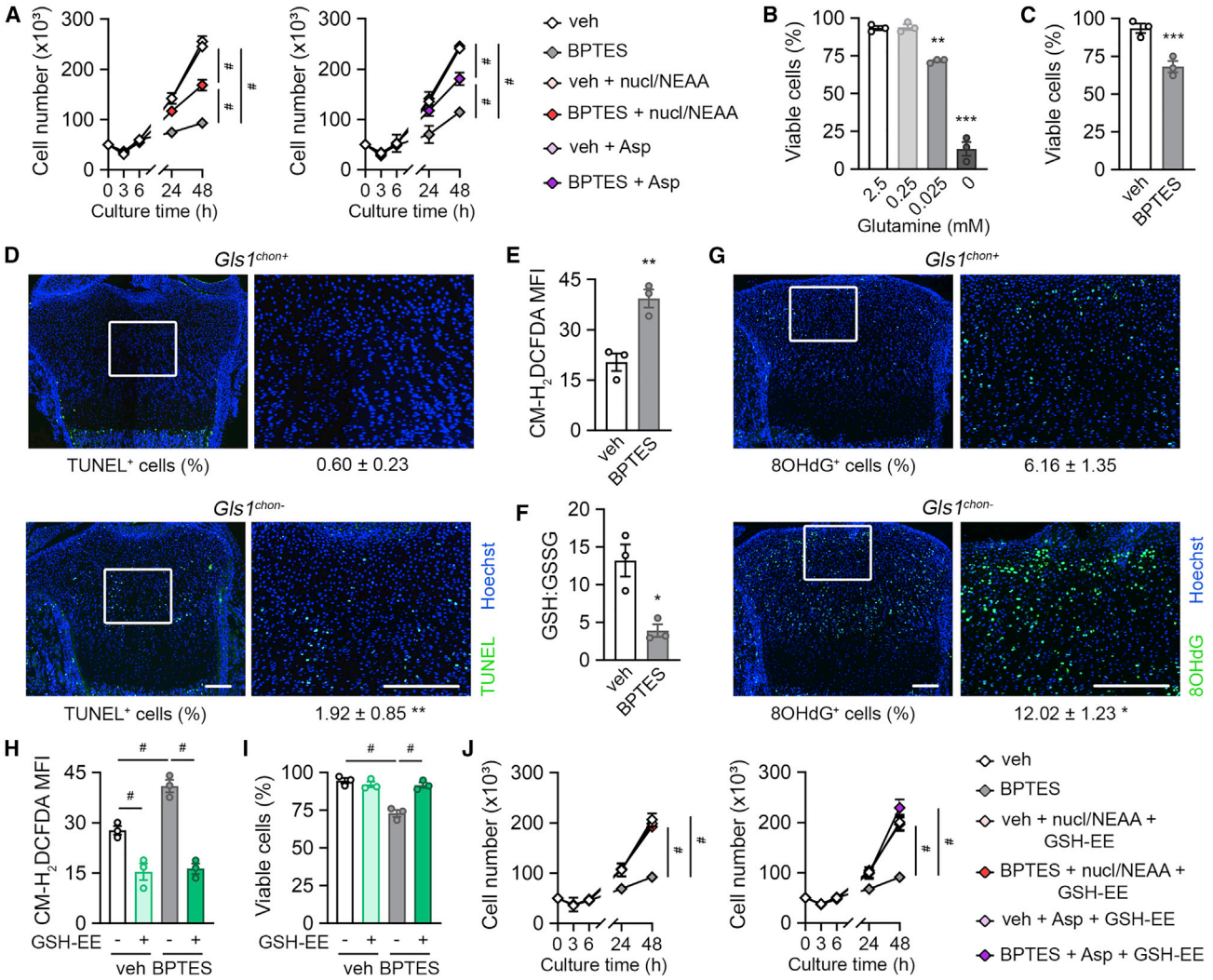

Figure 6. Chondrocytic Redox Homeostasis Depends on Glutamine-Dependent GSH Synthesis

(A) Growth curve of veh and BPTES-treated chondrocytes, with or without supplementation of nucleotides (nucl) and NEAA (left panel), or Asp (right panel) (n = 3).

(B and C) Viability of chondrocytes cultured in decreasing glutamine concentrations (B) or treated with BPTES (C), as determined by AnxV-PI flow cytometry (n = 3).

(D) TUNEL immunostaining of neonatal growth plates, with quantification of the percentage TUNEL-positive cells (n = 8). Boxed areas are magnified.

(E) Intracellular ROS levels, quantified as CM-H_2DCFDA MFI in veh or BPTES-treated chondrocytes (n = 3).

(F) Ratio of reduced glutathione (GSH) to oxidized glutathione (GSSG) (n = 6).

(G) 8-hydroxy-2′-deoxyguanosine (8OHdG) immunostaining of neonatal growth plates, with quantification of the percentage 8OHdG-positive cells (n = 8). Boxed areas are magnified.

(H and I) Intracellular ROS levels (H) and cell viability (I) of veh and BPTES-treated chondrocytes, with or without supplementation of glutathione ethyl ester (GSH-EE) (n = 3).

(J) Growth curve of veh and BPTES-treated chondrocytes, with or without supplementation of GSH-EE together with nucl and NEAA (left panel), or Asp (right panel) (n = 3).

Data are means ± SEM (A–C, E, F, and H–J) or means ± SD (E and H), *p < 0.05 versus 2.5 mM or veh or *Gls1*$^{chon+}$, **p < 0.01 versus 2.5 mM or veh or *Gls1*$^{chon+}$, ***p < 0.001 versus 2.5 mM or veh or *Gls1*$^{chon+}$ (Student's t-test), #p < 0.05 (ANOVA). Scale bars in (D) and (G) are 200 μm. See also Figure S6.

functions in chondrocytes. Indeed, both glutamine withdrawal and BPTES treatment decreased chondrocyte viability; an effect that was also observed in *Gls1*$^{chon-}$ mice (Figures 6B–6D).

To explore the underlying mechanism, we focused on glutathione synthesis as we have recently shown that glutamine-dependent glutathione production is necessary for adequate reactive oxygen species (ROS) scavenging and cell survival during bone repair (Stegen et al., 2016b). In line with these results, intracellular ROS levels were increased in BPTES-treated chondrocytes (Figure 6E), which was not caused by decreased expression of known ROS scavengers, such as superoxide dismutase (SOD) or catalase (Figure S6A) but rather by impaired glutathione synthesis. Indeed, levels of reduced glutathione (GSH), and consequently the ratio between GSH and oxidized

glutathione (GSSG) and the total glutathione pool, were significantly decreased in BPTES-treated cells (Figures 6F and S6B). We could not detect changes in enzymes involved in glutathione synthesis and/or recycling nor in reducing equivalents, but the GSH precursor amino acids glutamate and glycine were decreased (Figures S6C–S6E), indicating that the supply of metabolic substrates for GSH synthesis was impaired.

Accumulating ROS generate oxidative damage to cellular organelles, resulting in cell death (Schieber and Chandel, 2014). In agreement, we found that the increase in chondrocyte death was associated with manifest accumulation of oxidative DNA damage in *Gls1*$^{chon-}$ growth plates, as shown by 8-hydroxy-2′-deoxyguanosine immunostaining (Figure 6G). To prove the contribution of reduced glutathione levels to impaired redox homeostasis and cell survival, we treated chondrocytes with a cell-permeable glutathione ethyl ester (GSH-EE). This approach prevented the accumulation of intracellular ROS in vehicle and BPTES-treated cells and rescued the decrease in cell survival after inhibition of GLS1 (Figures 6H and 6I). Thus, glutamine catabolism via GLS1 is essential for chondrocytic redox homeostasis by controlling glutathione synthesis.

The glutamine-mediated maintenance of redox balance relied on other metabolic pathways than the ones that control biosynthesis, since restoring GSH levels in BPTES-treated chondrocytes did not alter proliferation and matrix synthesis, nor did normalizing biomass production affect cell survival or ROS levels (Figures S6F–S6M). Accordingly, simultaneous restoration of redox homeostasis and biosynthesis fully normalized the growth defect of BPTES-treated chondrocytes (Figures 6J and S6N–S6W).

In Vivo Validation of the Role of Glutamine Metabolism for Chondrocyte Function

Since a combination of glutamine-derived metabolites rescued the phenotypic defects upon GLS1 inhibition *in vitro*, we explored whether a similar strategy would also be successful in *Gls1*$^{chon-}$ mice. We first determined whether restoring acetyl-CoA synthesis would rescue the gene expression defect. In line with our *in vitro* observations, *in vivo* administration of acetate to newborn mice normalized chondrogenic gene expression in mutant growth plates to levels observed in vehicle-treated wild-type mice but did not rescue the reduced growth (Figures 7A and S7A). Next, we investigated whether restoration of chondrocyte biosynthesis in mutant mice would rescue the defect in proliferation and extracellular matrix synthesis. Aspartate supplementation restored biosynthesis in BPTES-treated chondrocytes (Figures 5B and 5C), but the need of such a supra-physiological concentration precludes a similar rescue experiment *in vivo*. As an alternative we used dimethyl-αKG, a cell-permeable glutamine-derived metabolite. In wild-type mice, αKG treatment had no effect on chondrocyte function, but it normalized the impaired growth as well as the decrease in chondrogenic gene expression in *Gls1*$^{chon-}$ mice (Figures 7B and 7C). Mechanistically, these beneficial effects on biosynthesis and gene expression were caused by a dual mechanism, whereby αKG supplementation (1) increased the levels of amino acids and nucleotides, thereby restoring proliferation and matrix deposition, and (2) restored acetyl-CoA levels and consequent histone acetylation, explaining the rescue in gene expression (Figures 7D–7H and S7B).

However, administration of αKG did not improve the survival of BPTES-treated chondrocytes, correlating with the lack of rescue of intracellular glutathione levels (Figures 7D and 7I). On the other hand, treating mutant mice with GSH-EE normalized the cell death phenotype (Figure 7J), likely by restoring redox homeostasis. In line with our *in vitro* observations, simultaneous administration of αKG and GSH-EE fully normalized the phenotype of *Gls1*$^{chon-}$ mice, evidenced by normalized chondrogenic gene expression, tibia length, and chondrocyte survival (Figures 7B, 7C, and 7J).

Finally, since endochondral fracture healing reiterates the sequence of events observed during development, we tested whether glutamine metabolism is involved in bone repair. Next to BPTES we also used the GLS1 inhibitor CB-839, which results in the same *in vitro* phenotypic effect as BPTES or genetic GLS1 inactivation (Figures S7C–S7G). Local injection of BPTES or CB-839 in a fracture callus decreased the presence of COL2-positive cartilage without affecting woven bone areas (Figures 7K and S7H), indicating that GLS1 regulates chondrocyte function during fracture healing.

DISCUSSION

Chondrocytes survive, proliferate, and deposit extracellular matrix in an avascular environment (Kronenberg, 2003; Long and Ornitz, 2013; Stegen and Carmeliet, 2019), yet the nutritional requirements for these functions are poorly characterized. Recent studies suggest that glucose regulates chondrocyte proliferation and matrix deposition (Lee et al., 2018; Stegen et al., 2019), although the exact metabolic link remains elusive. Likely, glucose is catabolized via glycolysis to support ATP production, although glucose oxidation is required for optimal energy homeostasis (Hollander and Zeng, 2019; Stegen et al., 2019; Tchetina and Markova, 2018). These observations suggest that other nutrients may have a complementary role to support chondrocyte function. Our recent work shows that chondrocytes are minimally dependent on exogenous fatty acids for bioenergetics and biosynthesis (van Gastel et al., 2020). In this study, we identify glutamine as a crucial metabolic regulator of chondrocyte identity and function during endochondral ossification as part of a feedforward process. In chondrocytes, SOX9 stimulates glutamine metabolism and this metabolic rewiring is in turn critical for chondrocyte gene expression, anabolism, and survival, highlighting the importance of metabolic specifications for chondrocyte function.

Skeletal progenitor cells in the developing limb bud differentiate into chondrocytes predominantly through the action of the transcription factor SOX9, which binds to hundreds of cartilage-specific genes (Kronenberg, 2003; Lefebvre et al., 2019; Long and Ornitz, 2013). We now show that SOX9 concurrently stimulates glutamine metabolism, revealing a metabolic role for the master chondrogenic transcription factor. Based on a SOX9 ChIP-seq dataset (Ohba et al., 2015), we could show SOX9 binding to the enhancer region of genes involved in glutamine metabolism. This metabolic adaptation is functionally important, as inhibiting glutamine metabolism in growth plate chondrocytes by deleting *Gls1* interferes with proper chondrocyte functioning and results in stunted long bone growth.

Mechanistically, glutamine metabolism regulates chondrocyte function by three different processes, each supported by a

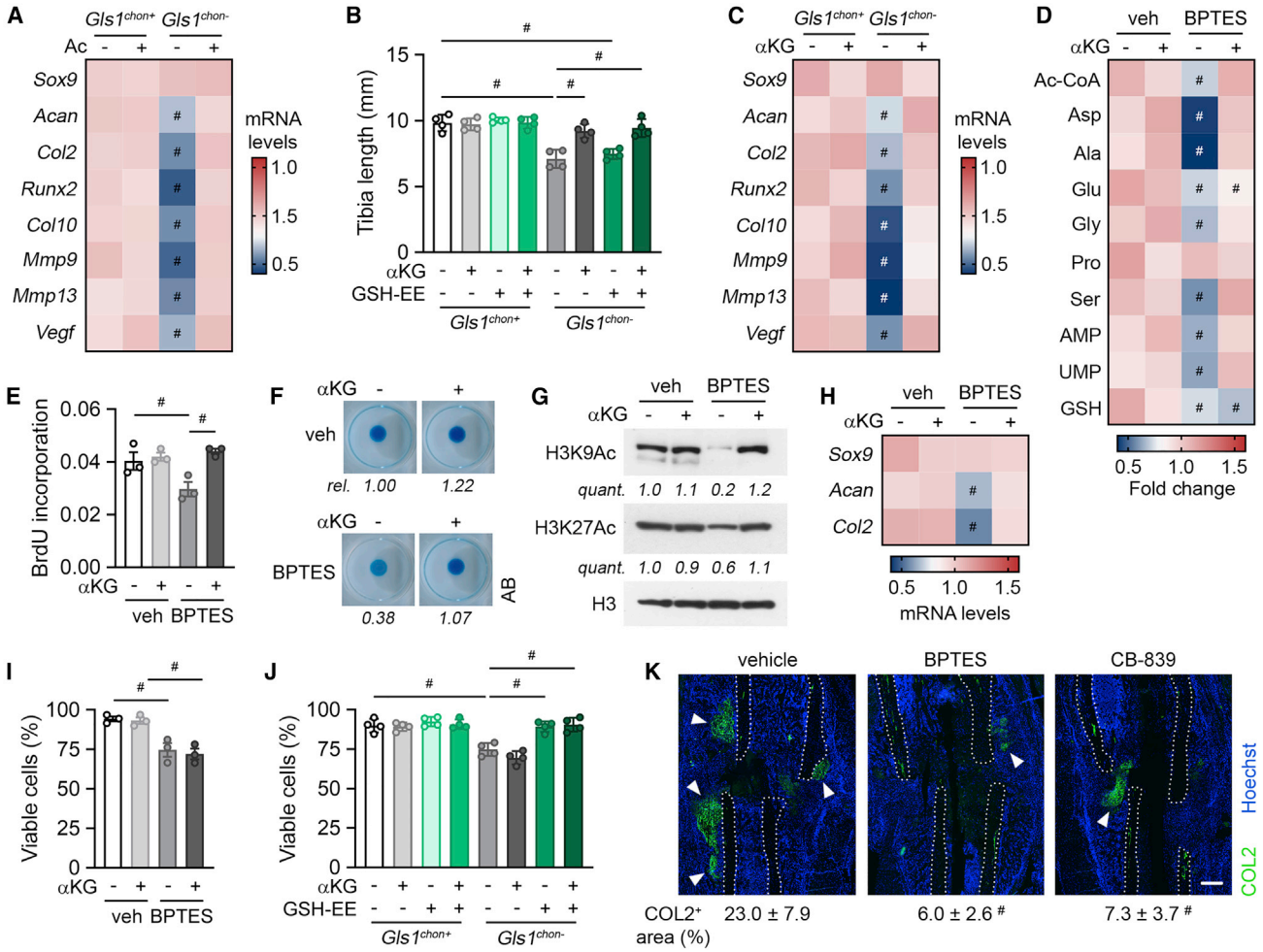

Figure 7. Combined Supplementation of αKG and GSH-EE *In Vivo* Rescues the *Gls1*$^{chon-}$ Phenotype

(A) *Sox9*, *Acan*, *Col2*, *Runx2*, *Col10*, *Mmp9*, *Mmp13*, and *Vegf* mRNA levels in growth plates derived from mice treated with Ac (n = 5).

(B) Tibia length of wild-type (*Gls1*$^{chon+}$) and chondrocyte-specific GLS1-deficient (*Gls1*$^{chon-}$) mice with or without αKG and GSH-EE treatment (n = 4).

(C) Chondrogenic gene expression in *Gls1*$^{chon+}$ and *Gls1*$^{chon-}$ mice with or without αKG treatment (n = 4).

(D) Intracellular Ac-CoA, Asp, Ala, Glu, Gly, Pro, Ser, purine (AMP), pyrimidine (UMP), and GSH levels in veh and BPTES-treated chondrocytes, with or without αKG supplementation (n = 3).

(E–I) Proliferation (E), matrix deposition in micromasses (F), immunoblot of H3K9Ac, H3K27Ac, and H3 levels (G), chondrogenic gene expression (H), and cell viability (I) in veh and BPTES-treated chondrocytes, with or without αKG supplementation (n = 3).

(J) Chondrocyte survival, quantified by *ex vivo* annexin V - propidium iodide flow cytometry, in *Gls1*$^{chon+}$ and *Gls1*$^{chon-}$ mice with or without αKG and GSH-EE treatment (n = 4).

(K) COL2 immunostaining with quantification of the COL2-positive area in the callus at post-fracture day 7 of vehicle, BPTES or CB-839-treated mice (n = 4). Scale bar is 250 μm, white arrowheads indicate COL2-positive cartilage.

Data are means ± SD (A, J, and K) or means ± SEM (E and I), #p < 0.05 (ANOVA). See also Figure S7.

different glutamine-metabolizing pathway. First, glutamine metabolism has a crucial role in the epigenetic control of SOX9-regulated chondrogenic genes. Histone acetylation of the enhancer region of chondrogenic genes, like *Acan* and *Col2*, renders the condensed chromatin into a more relaxed state and thereby promotes SOX9 access to these sites and thus chondrogenic gene transcription (Furumatsu and Asahara, 2010; Kinnaird et al., 2016; Ohba et al., 2015). Our data clearly demonstrate that glutamine, via GLUD1-dependent reductive carboxylation, is a critical nutritional source for acetyl-CoA, necessary for maintaining histone acetylation specifically in chondrogenic gene enhancer regions. Addition of acetate could rescue the decrease in chondrogenic gene expression *in vitro* and *in vivo*, indicating that other endogenous nutrients could not compensate the reduced acetyl-CoA levels when glutamine metabolism was impaired. These findings indicate that SOX9, by inducing glutamine metabolism, ensures optimal access to the SOX9-binding sites in order to induce chondrogenic gene expression.

Second, glutamine metabolism supports biosynthetic processes in chondrocytes, since impaired glutamine metabolism decreased proliferation and protein synthesis. This effect is

accompanied by reduced nucleotide and amino acid levels, but not by an energy deficit, which is in line with our previous study showing that glycolysis and glucose oxidation are the major energy-generating pathways in chondrocytes (Stegen et al., 2019). Recently, skeletal stem cells have been shown to rely on glutamine metabolism to support proliferation (Yu et al., 2019), although the precise mechanism was not investigated. Here, we show that chondrocytes meet their high anabolic demand through GOT2-dependent aspartate production, which in turn is necessary for DNA replication and protein synthesis. Importantly, GLUD1-driven glutamine flux into the TCA cycle is dispensable for maintaining chondrocyte biosynthetic processes, which is consistent with the fact that highly anabolic cells often rely more on transaminase rather than glutamate dehydrogenase activity (Coloff et al., 2016; Son et al., 2013).

Third, in line with our previous observations in skeletal progenitors (Stegen et al., 2016b), glutamine serves as a precursor metabolite for GSH synthesis to maintain redox homeostasis and cell viability. Indeed, inactivation of GLS1 or glutamine deprivation markedly increased ROS levels and chondrocyte death, which was rescued upon addition of a cell-permeable GSH analog.

Taken together, glutamine metabolism is important for chondrocyte identity and function during bone development and likely also during bone repair. Importantly, the flux of glutamine into anabolic pathways has to be tightly regulated, since inappropriately high GLS1-driven αKG synthesis stimulates collagen hydroxylation, resulting in heavily cross-linked collagen and ultimately skeletal dysplasia (Stegen et al., 2019). Whether alterations in glutamine metabolism are linked to other cartilage-related pathologies, including osteoarthritis, is an interesting question that requires further study.

STAR★METHODS

Detailed methods are provided in the online version of this paper and include the following:

SUPPLEMENTAL INFORMATION

Supplemental Information can be found online at https://doi.org/10.1016/j.devcel.2020.05.001.

ACKNOWLEDGMENTS

The authors wish to thank R. Van Looveren and S. Torrekens for technical assistance. G.C. acknowledges funding from the Research Foundation - Flanders (FWO: G.0964.14, G.0A42.16 and G.0B3418) and from KU Leuven (C24/17/077); P.C. from long-term structural funding – Methusalem Funding by the Flemish Government; S.-M.F. FWO research projects and KU Leuven Methusalem co-funding. S.S. and S.L. are research fellows from the FWO (12H5917N and 1S46318N). G.R. is supported by consecutive PhD fellowships from the Emmanuel van der Schueren - Kom op tegen Kanker foundation and FWO (1137117N and 1137119N). The authors declare no conflict of interest.

AUTHOR CONTRIBUTIONS

Conceptualization, S.S. and G.C.; Investigation, S.S., G.R., S.L., I.S., K.M., and B.T.; Resources, S.-M.F. and P.C.; Funding Acquisition, S.S. and G.C.; Writing – Original Draft, S.S. and G.C.; Supervision, G.C.

DECLARATION OF INTERESTS

The authors declare no competing interests.

Received: September 10, 2019
Revised: April 20, 2020
Accepted: May 1, 2020
Published: May 28, 2020

REFERENCES

Altman, B.J., Stine, Z.E., and Dang, C.V. (2016). From Krebs to clinic: glutamine metabolism to cancer therapy. Nat. Rev. Cancer *16*, 619–634.

Baron, J., Sävendahl, L., De Luca, F., Dauber, A., Phillip, M., Wit, J.M., and Nilsson, O. (2015). Short and tall stature: a new paradigm emerges. Nat. Rev. Endocrinol. *11*, 735–746.

Buescher, J.M., Antoniewicz, M.R., Boros, L.G., Burgess, S.C., Brunengraber, H., Clish, C.B., DeBerardinis, R.J., Feron, O., Frezza, C., Ghesquiere, B., et al. (2015). A roadmap for interpreting (13)C metabolite labeling patterns from cells. Curr. Opin. Biotechnol. *34*, 189–201.

Caballero, F., Fernández, A., Matías, N., Martínez, L., Fucho, R., Elena, M., Caballeria, J., Morales, A., Fernández-Checa, J.C., and García-Ruiz, C. (2010). Specific contribution of methionine and choline in nutritional nonalcoholic steatohepatitis: impact on mitochondrial S-adenosyl-L-methionine and glutathione. J. Biol. Chem. *285*, 18528–18536.

Chyu, K.Y., Babbidge, S.M., Zhao, X., Dandillaya, R., Rietveld, A.G., Yano, J., Dimayuga, P., Cercek, B., and Shah, P.K. (2004). Differential effects of green tea-derived catechin on developing versus established atherosclerosis in apolipoprotein E-null mice. Circulation *109*, 2448–2453.

Coloff, J.L., Murphy, J.P., Braun, C.R., Harris, I.S., Shelton, L.M., Kami, K., Gygi, S.P., Selfors, L.M., and Brugge, J.S. (2016). Differential glutamate metabolism in proliferating and quiescent mammary epithelial cells. Cell Metab. *23*, 867–880.

DeBerardinis, R.J., and Cheng, T. (2010). Q's next: the diverse functions of glutamine in metabolism, cell biology and cancer. Oncogene *29*, 313–324.

Elia, I., Broekaert, D., Christen, S., Boon, R., Radaelli, E., Orth, M.F., Verfaillie, C., Grünewald, T.G.P., and Fendt, S.M. (2017). Proline metabolism supports metastasis formation and could be inhibited to selectively target metastasizing cancer cells. Nat. Commun. *8*, 15267.

Frost, G., Sleeth, M.L., Sahuri-Arisoylu, M., Lizarbe, B., Cerdan, S., Brody, L., Anastasovska, J., Ghourab, S., Hankir, M., Zhang, S., et al. (2014). The short-chain fatty acid acetate reduces appetite via a central homeostatic mechanism. Nat. Commun. *5*, 3611.

Furumatsu, T., and Asahara, H. (2010). Histone acetylation influences the activity of Sox9-related transcriptional complex. Acta Med. Okayama *64*, 351–357.

Gao, P., Tchernyshyov, I., Chang, T.C., Lee, Y.S., Kita, K., Ochi, T., Zeller, K.I., De Marzo, A.M., Van Eyk, J.E., Mendell, J.T., and Dang, C.V. (2009). c-Myc suppression of miR-23a/b enhances mitochondrial glutaminase expression and glutamine metabolism. Nature *458*, 762–765.

Gaude, E., and Frezza, C. (2016). Tissue-specific and convergent metabolic transformation of cancer correlates with metastatic potential and patient survival. Nat. Commun. *7*, 13041.

Guo, W., Keckesova, Z., Donaher, J.L., Shibue, T., Tischler, V., Reinhardt, F., Itzkovitz, S., Noske, A., Zürrer-Härdi, U., Bell, G., et al. (2012). Slug and Sox9 cooperatively determine the mammary stem cell state. Cell *148*, 1015–1028.

Herlofsen, S.R., Bryne, J.C., Høiby, T., Wang, L., Issner, R., Zhang, X., Coyne, M.J., Boyle, P., Gu, H., Meza-Zepeda, L.A., et al. (2013). Genome-wide map of quantified epigenetic changes during in vitro chondrogenic differentiation of primary human mesenchymal stem cells. BMC Genomics *14*, 105.

Hollander, J.M., and Zeng, L. (2019). The emerging role of glucose metabolism in cartilage development. Curr. Osteoporos. Rep. *17*, 59–69.

Kinnaird, A., Zhao, S., Wellen, K.E., and Michelakis, E.D. (2016). Metabolic control of epigenetics in cancer. Nat. Rev. Cancer *16*, 694–707.

Kronenberg, H.M. (2003). Developmental regulation of the growth plate. Nature *423*, 332–336.

Lane, A.N., and Fan, T.W. (2015). Regulation of mammalian nucleotide metabolism and biosynthesis. Nucleic Acids Res. *43*, 2466–2485.

Lee, S.Y., Abel, E.D., and Long, F. (2018). Glucose metabolism induced by Bmp signaling is essential for murine skeletal development. Nat. Commun. *9*, 4831.

Lefebvre, V., Angelozzi, M., and Haseeb, A. (2019). SOX9 in cartilage development and disease. Curr. Opin. Cell Biol. *61*, 39–47.

Long, F., and Ornitz, D.M. (2013). Development of the endochondral skeleton. Cold Spring Harb. Perspect. Biol. *5*, a008334.

Lorendeau, D., Rinaldi, G., Boon, R., Spincemaille, P., Metzger, K., Jäger, C., Christen, S., Dong, X., Kuenen, S., Voordeckers, K., et al. (2017). Dual loss of succinate dehydrogenase (SDH) and complex I activity is necessary to recapitulate the metabolic phenotype of SDH mutant tumors. Metab. Eng. *43*, 187–197.

Maes, C., Araldi, E., Haigh, K., Khatri, R., Van Looveren, R., Giaccia, A.J., Haigh, J.J., Carmeliet, G., and Schipani, E. (2012). VEGF-independent cell-autonomous functions of HIF-1alpha regulating oxygen consumption in fetal cartilage are critical for chondrocyte survival. J. Bone Miner. Res. *27*, 596–609.

Maes, C., Coenegrachts, L., Stockmans, I., Daci, E., Luttun, A., Petryk, A., Gopalakrishnan, R., Moermans, K., Smets, N., Verfaillie, C.M., et al. (2006). Placental growth factor mediates mesenchymal cell development, cartilage turnover, and bone remodeling during fracture repair. J. Clin. Invest. *116*, 1230–1242.

Mingote, S., Masson, J., Gellman, C., Thomsen, G.M., Lin, C.S., Merker, R.J., Gaisler-Salomon, I., Wang, Y., Ernst, R., Hen, R., and Rayport, S. (2015). Genetic pharmacotherapy as an early CNS drug development strategy: testing glutaminase inhibition for schizophrenia treatment in adult mice. Front. Syst. Neurosci. *9*, 165.

Ohba, S., He, X., Hojo, H., and McMahon, A.P. (2015). Distinct transcriptional programs underlie Sox9 regulation of the mammalian chondrocyte. Cell Rep. *12*, 229–243.

Ovchinnikov, D.A., Deng, J.M., Ogunrinu, G., and Behringer, R.R. (2000). Col2a1-directed expression of Cre recombinase in differentiating chondrocytes in transgenic mice. Genesis *26*, 145–146.

Rajeshkumar, N.V., Yabuuchi, S., Pai, S.G., De Oliveira, E., Kamphorst, J.J., Rabinowitz, J.D., Tejero, H., Al-Shahrour, F., Hidalgo, M., Maitra, A., and Dang, C.V. (2017). Treatment of pancreatic cancer patient-derived Xenograft Panel with metabolic inhibitors reveals efficacy of phenformin. Clin. Cancer Res. *23*, 5639–5647.

Reid, M.A., Dai, Z., and Locasale, J.W. (2017). The impact of cellular metabolism on chromatin dynamics and epigenetics. Nat. Cell Biol. *19*, 1298–1306.

Ruan, J.J., Yu, Y., Hou, W., Chen, Z., Fang, J., Zhang, J., Ni, M., Li, D., Lu, S., Rui, J., et al. (2019). Kidney-type glutaminase inhibitor Hexylselen selectively kills cancer cells via a three-pronged mechanism. ACS Pharmacol. Transl. Sci. *2*, 18–30.

Sanjana, N.M., Shalem, O., and Zhang, F. (2014). Improved vectors and genome-wide libraries for CRISPR screening. Nat Methods *11*, 783–784.

Schieber, M., and Chandel, N.S. (2014). ROS function in redox signaling and oxidative stress. Curr. Biol. *24*, R453–R462.

Sivanand, S., Viney, I., and Wellen, K.E. (2018). Spatiotemporal control of acetyl-CoA metabolism in chromatin regulation. Trends Biochem. Sci. *43*, 61–74.

Son, J., Lyssiotis, C.A., Ying, H., Wang, X., Hua, S., Ligorio, M., Perera, R.M., Ferrone, C.R., Mullarky, E., Shyh-Chang, N., et al. (2013). Glutamine supports pancreatic cancer growth through a KRAS-regulated metabolic pathway. Nature *496*, 101–105.

Speight, G., Handley, C.J., and Lowther, D.A. (1978). Extracellular matrix metabolism by chondrocytes. 4. Role of glutamine in glycosaminoglycan synthesis in vitro by chondrocytes. Biochim. Biophys. Acta *540*, 238–245.

Stegen, S., and Carmeliet, G. (2019). Hypoxia, hypoxia-inducible transcription factors and oxygen-sensing prolyl hydroxylases in bone development and homeostasis. Curr. Opin. Nephrol. Hypertens. *28*, 328–335.

Stegen, S., Deprez, S., Eelen, G., Torrekens, S., Van Looveren, R., Goveia, J., Ghesquière, B., Carmeliet, P., and Carmeliet, G. (2016a). Adequate hypoxia inducible factor 1alpha signaling is indispensable for bone regeneration. Bone *87*, 176–186.

Stegen, S., Laperre, K., Eelen, G., Rinaldi, G., Fraisl, P., Torrekens, S., Van Looveren, R., Loopmans, S., Bultynck, G., Vinckier, S., et al. (2019). HIF-1alpha metabolically controls collagen synthesis and modification in chondrocytes. Nature *565*, 511–515.

Stegen, S., Stockmans, I., Moermans, K., Thienpont, B., Maxwell, P.H., Carmeliet, P., and Carmeliet, G. (2018). Osteocytic oxygen sensing controls bone mass through epigenetic regulation of sclerostin. Nat. Commun. *9*, 2557.

Stegen, S., van Gastel, N., Eelen, G., Ghesquière, B., D'Anna, F., Thienpont, B., Goveia, J., Torrekens, S., Van Looveren, R., Luyten, F.P., et al. (2016b). HIF-1alpha promotes glutamine-mediated redox homeostasis and glycogen-dependent bioenergetics to support postimplantation bone cell survival. Cell Metab. *23*, 265–279.

Stine, Z.E., Walton, Z.E., Altman, B.J., Hsieh, A.L., and Dang, C.V. (2015). MYC, metabolism, and cancer. Cancer Discov. *5*, 1024–1039.

Sullivan, M.R., and Vander Heiden, M.G. (2019). Determinants of nutrient limitation in cancer. Crit. Rev. Biochem. Mol. Biol. *54*, 193–207.

Tchetina, E.V., and Markova, G.A. (2018). Regulation of energy metabolism in the growth plate and osteoarthritic chondrocytes. Rheumatol. Int. *38*, 1963–1974.

van Gastel, N., Stegen, S., Eelen, G., Schoors, S., Carlier, A., Daniëls, V.W., Baryawno, N., Przybylski, D., Depypere, M., Stiers, P.J., et al. (2020). Lipid availability determines fate of skeletal progenitor cells via SOX9. Nature *579*, 111–117.

van Gastel, N., Stegen, S., Stockmans, I., Moermans, K., Schrooten, J., Graf, D., Luyten, F.P., and Carmeliet, G. (2014). Expansion of murine periosteal progenitor cells with fibroblast growth factor 2 reveals an intrinsic endochondral

ossification program mediated by bone morphogenetic protein 2. Stem Cells *32*, 2407–2418.

van Gastel, N., Torrekens, S., Roberts, S.J., Moermans, K., Schrooten, J., Carmeliet, P., Luttun, A., Luyten, F.P., and Carmeliet, G. (2012). Engineering vascularized bone: osteogenic and proangiogenic potential of murine periosteal cells. Stem Cells *30*, 2460–2471.

Vander Heiden, M.G., and DeBerardinis, R.J. (2017). Understanding the intersections between metabolism and cancer biology. Cell *168*, 657–669.

Yu, Y., Newman, H., Shen, L., Sharma, D., Hu, G., Mirando, A.J., Zhang, H., Knudsen, E., Zhang, G.F., Hilton, M.J., and Karner, C.M. (2019). Glutamine metabolism regulates proliferation and lineage allocation in skeletal stem cells. Cell Metab. *29*, 966–978.e4.

Zhang, J., Pavlova, N.N., and Thompson, C.B. (2017). Cancer cell metabolism: the essential role of the nonessential amino acid, glutamine. EMBO J. *36*, 1302–1315.

Zhou, Z.Q., Shung, C.Y., Ota, S., Akiyama, H., Keene, D.R., and Hurlin, P.J. (2011). Sequential and coordinated actions of c-Myc and N-Myc control appendicular skeletal development. PLoS One *6*, e18795.

Zhu, J., and Thompson, C.B. (2019). Metabolic regulation of cell growth and proliferation. Nat. Rev. Mol. Cell Biol. *20*, 436–450.

STAR★METHODS

KEY RESOURCES TABLE

REAGENT or RESOURCE	SOURCE	IDENTIFIER
Antibodies - Western blot		
Rabbit polyclonal anti-AMPKα	Cell Signaling Technology	Cat# 2532; RRID: AB_330331
Rabbit monoclonal anti-phospho-AMPKα (Thr172)	Cell Signaling Technology	Cat# 2535 (40H9); RRID: AB_331250
Mouse monoclonal anti-β-actin	Sigma-Aldrich	Cat# A5441 (AC-15); RRID: AB_476744
Rabbit monoclonal anti-c-Myc	Cell Signaling Technology	Cat# 5605 (D84C12); RRID: AB_1903938
Rabbit polyclonal anti-GLS1	Abcam	Cat# ab93434; RRID: AB_10561964
Rabbit monoclonal anti-GLUD1	Abcam	Cat# ab166618 (EPR11369(B)); RRID: AB_2815030
Rabbit monoclonal anti-GOT2	Abcam	Cat# ab171739 (EPR12354(B))
Rabbit monoclonal anti-histone H2A	Cell Signaling Technology	Cat# 12349 (D6O3A); RRID: AB_2687875
Rabbit polyclonal anti-acetyl-histone H2A (Lys5)	Cell Signaling Technology	Cat# 2576; RRID: AB_2118805
Rabbit monoclonal anti-histone H3	Cell Signaling Technology	Cat# 4499 (D1H2); RRID: AB_10544537
Rabbit monoclonal anti-acetyl-histone H3 (Lys9)	Cell Signaling Technology	Cat# 9649 (C5B11); RRID: AB_823528
Rabbit monoclonal anti-acetyl-histone H3 (Lys14)	Cell Signaling Technology	Cat# 7627 (D4B9); RRID: AB_10839410
Rabbit monoclonal anti-acetyl-histone H3 (Lys27)	Cell Signaling Technology	Cat# 8173 (D5E4); RRID: AB_10949503
Rabbit monoclonal anti-dimethyl-histone H3 (Lys9)	Abcam	Cat# ab176882 (EP16990)
Rabbit monoclonal anti-trimethyl H3 (Lys27)	Abcam	Cat# ab192985 (EPR18607); RRID: AB_2650559
Rabbit monoclonal anti-histone H4	Cell Signaling Technology	Cat# 13919 (D2X4V); RRID: AB_2798345
Rabbit monoclonal anti-acetyl-histone H4 (Lys4)	Abcam	Cat# ab176799 (EPR16596)
Rabbit monoclonal anti-acetyl-histone H4 (Lys8)	Cell Signaling Technology	Cat# 2594; RRID: AB_2248400
Rabbit polyclonal anti-5-hydroxymethylcytosine	Active Motif	Cat# 39769; RRID: AB_10013602
Rabbit polyclonal anti-SOX9	Bio-Techne	Cat# NBP1-85551; RRID: AB_11002706
Antibodies - Immunohistochemistry		
Goat polyclonal anti-8-hydroxyguanosine	Abcam	Cat# ab10802; RRID: AB_297482
Rabbit polyclonal anti-Ki67	Leica Biosystems	Cat# NCL-Ki67p; RRID: AB_442102
Mouse monoclonal anti-type 2 collagen	Chemicon	Cat# MAB8887; RRID: AB_2260779
Antibodies - ChIP-qPCR		
Normal rabbit IgG	Cell Signaling Technology	Cat# 2729; RRID: AB_1031062
Chemicals, Peptides, and Recombinant Proteins		
$^{13}C_6$-glucose	Cambridge Isotope Laboratories	Cat# CLM-1396
$^{13}C_5$-glutamine	Cambridge Isotope Laboratories	Cat# CLM-1822-H
$^{13}C_4{}^{15}N$-aspartate	Cambridge Isotope Laboratories	Cat# CNLM-544-H
^{3}H-proline	PerkinElmer	Cat# NET483001MC
5-^{13}C-glutamine	Cambridge Isotope Laboratories	Cat# CLM-1166
Alcian Blue 8GX	Sigma-Aldrich	Cat# A5268
Aminooxyacetate	Sigma-Aldrich	Cat# C13408
Bovine albumin serum	Sigma-Aldrich	Cat# A2153
Bis-2-(5-phenylacetamido-1,2,4-thiadiazol-2-yl)ethyl sulfide	Sigma-Aldrich	Cat# SML0601
CB-839	Selleckchem	Cat# S7655
Collagenase type II	Gibco	Cat# 17101015
cOmplete protease inhibitor cocktail	Roche	Cat# 11873580001
Dimethyl-α-ketoglutarate	Sigma-Aldrich	Cat# 349631
Dimethyl sulfoxide	Sigma-Aldrich	Cat# D8418
Dispase	Gibco	Cat# 17105041

(*Continued on next page*)

Continued

REAGENT or RESOURCE	SOURCE	IDENTIFIER
EmbryoMax Nucleoside mixture	Merck	Cat# ES-008-D
Epigallocatechin gallate	Sigma-Aldrich	Cat# E4143
Fetal bovine serum	Gibco	Cat# 10270106
Glutathione reduced ethyl ester	Sigma-Aldrich	Cat# 39073
Heparin	LEO Pharma	Cat# B01AB01
L-ascorbic acid 2-sulphate	Sigma-Aldrich	Cat# A92902
L-aspartic acid β-methyl ester hydrochloride	Sigma-Aldrich	Cat# A8291
Low melting point agarose	Lonza	Cat# 50115
MEM α, GlutaMAX™ Supplement, no nucleosides	Gibco	Cat# 32561029
MEM Non-Essential Amino Acids solution	Thermo Fisher Scientific	Cat# 11140050
Methoxyamine hydrochloride	Sigma-Aldrich	Cat# 226904
Mitomycin C	Sigma-Aldrich	Cat# MO503
N-(tert-butyldimethylsilyl)-N-methyl-trifluoroacetamide	Sigma-Aldrich	Cat# 394882
Penicillin/streptomycin	Gibco	Cat# 11548876
Polybrene	Sigma-Aldrich	Cat# TR-1003
PhosSTOP phosphatase inhibitor cocktail	Roche	Cat# 04906837001
Propidium iodide	Thermo Fisher Scientific	Cat# P3566
Rat tail type I collagen	Corning GmbH	Cat# 354236
Recombinant human fibroblast growth factor 2	R&D Systems	Cat# 233-FB
Recombinant human transforming growth factor-β1	Peprotech	Cat# 100-21
Saline-sodium citrate buffer 20x concentrate	Sigma-Aldrich	Cat# S6639
Sodium acetate	Sigma-Aldrich	Cat# 241245
Superscript II Reverse Transcriptase	Thermo Fisher Scientific	Cat# 18064022
SYBR GreenER qPCR SuperMix Universal	Thermo Fisher Scientific	Cat# 1178401K
tert-Butyldimethylchlorosilane	Sigma-Aldrich	Cat# 8.18642
Trichloroacetic acid	Sigma-Aldrich	Cat# T6399
Trichostatin A	Sigma-Aldrich	Cat# T8552
Triton X-100	Sigma-Aldrich	Cat# X100
Trypsin-EDTA (0.05%)	Gibco	Cat# 25300054
Western Lightning Plus-ECL, Enhanced Chemiluminescence Substrate	PerkinElmer	Cat# NEL103E001EA
Y-27632 (ROCK inhibitor)	Axon Medchem	Cat# 1683
Critical Commercial Assays		
Agencourt AMPure XP	Beckman Coulter	Cat# A63881
Antigen Retrieval Solution	Dako	Cat# S169984-2
BCA Protein Assay Reagent	Thermo Fisher Scientific	Cat# 23225
Cell Proliferation Biotrack ELISA system	GE Healthcare	Cat# RPN250
Click-iT® L-homopropargylglycine Alexa Fluor® 488 Protein Synthesis Assay Kit	Thermo Fisher Scientific	Cat# C10428
CM-H_2DCFDA	Thermo Fisher Scientific	Cat# C6827
Dead Cell Apoptosis Kit	Thermo Fisher Scientific	Cat# V13245
DNeasy Blood & Tissue Kit	QIAGEN	Cat# 69504
In Situ Cell Death Detection Kit	Roche	Cat# 11684795910
NucleoSpin RNA isolation kit	Machery Nagel	Cat# 740955
Pierce Protein A/G Magnetic Beads	Thermo Fisher Scientific	Cat# 88803
Experimental Models: Organisms/Strains		
Mouse: $Gls^{tm1Sray}$ (i.e. *Gls1*$^{fl/fl}$)	Mingote et al., 2015	N/A
Mouse: B6;SJL-Tg(Col2a1-cre)1Bhr/J (i.e. *Col2*-Cre)	Ovchinnikov et al., 2000	N/A

(*Continued on next page*)

Continued

REAGENT or RESOURCE	SOURCE	IDENTIFIER
Oligonucleotides		
Primer sequences for qRT-PCR - see Table S2	N/A	N/A
Gls1 sgRNA: 5'-AGTGCTAAAAAGCAGTCTGGAGG-3'	This paper	N/A
Glud1 sgRNA: 5'-AGGCTCAACACATGGTTGCAGGG-3'	This paper	N/A
Got2 sgRNA: 5'-AGGCTCAACACATGGTTGCAGGG-3'	This paper	N/A
GLS1 shRNA: CCGGGAGGGAAGGTTGCTGATTA TACTCGAGTATAATCAGCAACCTTCCCTCTTTTTG	Sigma-Aldrich	TRCN0000253167
GLUD1 shRNA: CCGGGAGAGTCTGATGGGAGTAT ATCTCGAGATATACTCCCATCAGACTCTCTTTTTG	Sigma-Aldrich	TRCN0000041505
GOT2 shRNA: CCGGGAGCCCTAGAAGACATATCA ACTCGAGTTGATATGTCTTCTAGGGCTCTTTTTG	Sigma-Aldrich	TRCN0000325946
c-MYC shRNA: CCGGTGGAGATGATGACCGAGTTA CCTCGAGGTAACTCGGTCATCATCTCCATTTTTG	Sigma-Aldrich	TRCN0000234925
Primer sequences for SOX9 binding motifs in the *Gls1* enhancer - see STAR Methods section	This paper	N/A
Primer sequences for SOX9 binding motifs in the *c-Myc* enhancer - see STAR Methods section	This paper	N/A
Primer sequences for H3K27Ac ChIP-qPCR - see STAR Methods section	This paper	N/A
Recombinant DNA		
SOX9 overexpression plasmid: pWPXL-Sox9	Guo et al., 2012	Addgene plasmid repository #36979
SOX9 knockdown plasmid: pLKO.1-sh-mSOX9-2	Guo et al., 2012	Addgene plasmid repository #40645
Cas9-expressing plasmid: lentiCRISPR v2	Sanjana et al., 2014	Addgene plasmid repository #52961
Software and Algorithms		
BedTools (version 2.26.0)	https://bedtools.readthedocs.io/en/latest/	N/A
GraphPad Prism (version 8.3.0)	http://www.graphpad.com/	N/A
NCSS statistical software	https://www.ncss.com/	N/A
Kaluza	https://www.beckman.com/flow-cytometry/software/kaluza	N/A
TopGO (version 1.0)	https://bioconductor.org/packages/release/bioc/html/topGO.html	N/A
Xcalibur Software	Thermo Fisher Scientific	N/A
Other		
Amersham Protran 0.45 nitrocellulose membrane	GE Healthcare	Cat# 10600002
BIOTRANS(+) nylon membrane	MP Biomedicals	Cat# ICN810205

RESOURCE AVAILABILITY

Lead Contact

Further information and requests for resources and reagents should be directed to and will be fulfilled, upon reasonable request, by the Lead Contact, Geert Carmeliet (geert.carmeliet@kuleuven.be).

Materials Availability

This study did not generate new unique reagents.

Data and Code Availability

This study did not generate any unique datasets or code.

EXPERIMENTAL MODEL AND SUBJECT DETAILS

Animals

Chondrocyte-specific deletion of GLS1 was obtained by crossing *Gls1*$^{fl/fl}$ mice (exon 1 was flanked by LoxP sites, mice were generated as described before (Mingote et al., 2015)) with transgenic mice expressing Cre recombinase under the control of the *type 2 collagen* (*Col2*) gene promoter (Ovchinnikov et al., 2000) (*Col2-Cre*$^{+}$ *Gls1*$^{fl/fl}$, referred to as *Gls1*$^{chon-}$). *Col2-Cre*$^{-}$ *Gls1*$^{fl/fl}$ (referred to as *Gls1*$^{chon+}$) littermates were used as control in all experiments; phenotypic analysis was performed on 3-day-old or 14-day-old male mice. Mice were bred in conventional conditions in our animal housing facility (Proefdierencentrum Leuven, Belgium). Housing and experimental procedures were approved by the Institutional Animal Care and Research Advisory Committee of the KU Leuven.

Ectopic Bone Ossicle Model

A recently described ectopic bone ossicle model was used as a model for endochondral ossification (Stegen et al., 2019; van Gastel et al., 2014). This model adequately reiterates the sequence of events that is observed during endochondral bone development, with subsequently the deposition of COL2-positive cartilaginous matrix, matrix resorption by invading osteoclasts and bone formation by osteoblasts (van Gastel et al., 2014). Briefly, skeletal progenitor cells were isolated from the periosteum as described above and cultured in αMEM with 2 mM glutaMAX-1, containing 10% FBS, 100 units/ml penicillin and 50 μg/ml streptomycin supplemented with 5 U/ml heparin (LEO Pharma) and 5 ng/ml human recombinant fibroblast growth factor 2 (FGF2) (R&D Systems) to induce chondrogenic differentiation after implantation. After expansion, genetically modified (as described above) FGF2-pretreated skeletal progenitors were embedded in a type I collagen gel (5 mg/ml in PBS; Corning GmbH) at a density of 1x10^{7} cells/ml, and 100 μl was injected subcutaneously at the shoulder region of 8-week-old mice. One week after implantation, the timepoint when the cartilaginous matrix is formed (van Gastel et al., 2014), ectopic implants were collected, and either directly used for RNA isolation, or fixed in 2% paraformaldehyde and processed for histological analysis. Implant volume was measured using a caliper and calculated using the formula:

$$V = \frac{W^2 \times L}{2}$$

where V is implant volume, W is implant width, and L is implant length.

Semi-stabilized Fracture Model

The tibial semi-stabilized fracture model was performed as previously described (Maes et al., 2006). Briefly, a transverse fracture was induced in the right tibia of 8-week-old male mice and semi-stabilized by an intramedullary fixating steel pin. Three days after fracture induction, mice were treated daily by subcutaneously injecting 50 μl of a BPTES (25 μg/g body weight) or CB-839 (10 μg/g body weight) solution in saline at the fracture site. A 0.2% DMSO in saline solution was used as vehicle control. At day 10 post-fracture, tibias were dissected, fixed in 2% paraformaldehyde and processed for histological analysis.

Cell culture

Cell Isolation

Primary growth plate chondrocytes were isolated as described before (Stegen et al., 2019). Briefly, chondrocytes were isolated from growth plates of the proximal tibia and distal femur of 5-day-old male and female mice. After removal of the perichondrium, isolated growth plates were pre-digested by constant agitation for 30 minutes at room temperature with 1 mg/ml collagenase type II (Gibco) dissolved in growth medium (αMEM with 2 mM glutaMAX-1, containing 100 units/ml penicillin, 50 μg/ml streptomycin and 10% fetal bovine serum (FBS); all from Gibco). The remaining growth plate fragments were subsequently digested in 2 mg/ml collagenase type II for 3 hours at 37°C. The cell suspension obtained by the second digest was filtered through a 40 μm nylon mesh and single cells were recovered by centrifugation. Primary chondrocytes were seeded at a density of 3x10^{4} cells/cm^{2} and medium was changed every other day. Upon 80% confluency, cells were trypsinized and seeded for experiments.

Skeletal progenitor cells were isolated from the periosteum of long bones of 7-to-9-week-old male mice (van Gastel et al., 2012). After removal of muscle and connective tissue, epiphyses were embedded in 5% low melting point agarose (Lonza). Subsequently, periosteal cells were isolated by a twofold collagenase-dispase digest (3 mg/ml collagenase and 4 mg/ml dispase in αMEM with 2 mM glutaMAX-1, containing 100 units/ml penicillin and 50 μg/ml streptomycin; all from Gibco). Cells obtained after 10 minutes of digest were discarded. The cells obtained during the second digest (50 minutes) were passed through a 70 μm nylon mesh, washed and plated in αMEM with 2 mM glutaMAX-1, containing 100 units/ml penicillin, 50 μg/ml streptomycin and 10% FBS at a density of 1x10^{4} cells/cm^{2}. Medium was changed every other day and upon 80% confluency cells were trypsinized and seeded for experiments.

Micromass Cultures

Micromass cultures were used to either investigate chondrogenic differentiation starting from skeletal progenitors, or to analyse matrix deposition by lineage-committed chondrocytes. To assess chondrogenic differentiation, skeletal progenitor cells were first treated with mitomycin C (50 ng/ml) for 30 minutes to inhibit proliferation. Next, 1.5x10^{5} cells were resuspended in 10 μl of growth medium (αMEM with 2 mM glutaMAX-1, containing 100 units/ml penicillin, 50 μg/ml streptomycin and 1% FBS) and seeded as micromasses. Cells were allowed to attach for 1 hour at 37°C, after which 0.5 ml of growth medium supplemented with 10 ng/ml

recombinant human transforming growth factor-β1 (Peprotech), 50 μM L-ascorbic acid 2-sulphate (Sigma-Aldrich) and 20 μM Y-27632 (ROCK inhibitor; Axon Medchem) was added to the wells (i.e. chondrogenic medium). Medium was refreshed every other day and after 9 days micromasses were either stained with Alcian Blue (van Gastel et al., 2012) or used for gene expression analyses. To assess matrix deposition, $1.5x10^5$ mitomycin-pretreated growth plate chondrocytes were seeded as micromasses as described above. After 5 days of culture in normal growth medium supplemented with 50 μM L-ascorbic acid 2-sulphate, micromasses were stained with Alcian Blue.

METHOD DETAILS

ChIP-seq Dataset Analysis

Class 2 peaks as defined by Ohba and colleagues (Ohba et al., 2015) were intersected with protein-coding genes as annotated in the human genome (Ensembl build 92) using BedTools (version 2.26.0), with peaks being uniquely assigned to the nearest annotated gene start site. The resulting gene list was collated to remove all duplicate entries, and compared to the lists of genes associated with 85 metabolic pathways, as defined by Gaude and Frezza (Gaude and Frezza, 2016), using topGO (version 1.0). Metabolic pathways associated with fewer than 5 genes were discarded. Significance of enrichment was assessed following the "classic" algorithm, using Fisher's Exact test, and corrected for multiple testing as proposed by Benjamini and Hochberg.

Genetic Targeting

To modulate SOX9 expression, we transduced skeletal progenitor cells or growth plate chondrocytes, in the presence of 8 μg/ml polybrene (Sigma-Aldrich), with a lentivirus carrying a SOX9-overexpression plasmid (Addgene plasmid repository #36979 (Guo et al., 2012); MOI 150) or a shRNA against SOX9 (Addgene plasmid repository #40645 (Guo et al., 2012); MOI 50), respectively. A nonsense scrambled shRNA sequence or empty viral vector was used as a negative control. For c-MYC knockdown, chondrocytes were transduced with a lentivirus carrying a shRNA against c-MYC (TRCN0000234925 from Sigma-Aldrich; MOI 50). After 24 hours, virus-containing medium was changed to normal culture medium and 48 hours later, cells were used for further experiments.

To silence GLS1, GLUD1 or GOT2 in skeletal progenitors or chondrocytes using CRISPR-Cas9, we transduced these cells with a lentivirus carrying a plasmid containing the Cas9 enzyme (lentiCRISPR v2; Addgene plasmid repository #52961) and a sgRNA against *Gls1* (5'- AGTGCTAAAAAGCAGTCTGGAGG-3'), *Glud1* (5'-AGGCTCAACACATGGTTGCAGGG-3') or *Got2* (5'-AGGCTCAACA CATGGTTGCAGGG-3'). A nonsense scrambled sgRNA was used as a negative control. After 24 hours, virus-containing medium was changed to normal culture medium and cells were selected with puromycin (0.3 μg/ml) for 7 days before they were used in subsequent experiments. The results obtained using CRISPR-Cas9-mediated knockdown were confirmed using shRNA against GLS1 (TRCN0000253167, Sigma-Aldrich), GLUD1 (TRCN0000041505, Sigma-Aldrich) or GOT2 (TRCN0000325946, Sigma-Aldrich) (data are available upon request).

Inhibitors and Intermediates of Metabolic Pathways

Bis-2-(5-phenylacetamido-1,2,4-thiadiazol-2-yl)ethyl sulfide (BPTES), sodium acetate, trichostatin A (TSA), L-aspartic acid β-methyl ester hydrochloride, epigallocatechin gallate (EGCG), aminooxyacetate (AOA), glutathione reduced ethyl ester (GSH-EE) and dimethyl-α-ketoglutarate (dimethyl-αKG) were obtained from Sigma-Aldrich. CB-839 was purchased from Selleckchem. MEM Non-Essential Amino Acids solution (100x) was from Thermo Fisher Scientific, EmbryoMax Nucleoside mixture (100x) was from Merck.

All *in vitro* treatments with BPTES were at 5 μM; TSA was used at 300 nM, EGCG was used at 100 μM, AOA was used at 0.5 mM, and dimethyl-αKG was used at 0.5 mM. Rescue experiments with sodium acetate and GSH-EE were performed at 1 mM, L-aspartic acid β-methyl ester hydrochloride was used at 20 mM, and a 1x NEAA or nucleoside mixture was used. Dose-response experiments were initially performed to determine a physiologically relevant concentration that does not induce cytotoxicity. For BPTES, TSA, EGCG, AOA and GSH-EE, dimethyl sulfoxide (DMSO) was used as vehicle control; sodium acetate, L-aspartic acid β-methyl ester hydrochloride, NEAA and nucleotide mixture were solubilized in culture medium. For sodium acetate and L-aspartic acid β-methyl ester hydrochloride, pH was adjusted with NaOH. Cells were treated for 3 days prior to analysis unless otherwise specified.

For *in vivo* studies, sodium acetate (500 μg/g body weight), EGCG (10 μg/g body weight), AOA (10 μg/g body weight), dimethyl-αKG (50 μg/g body weight) or GSH-EE (420 μg/g body weight) were administered to newborn mice daily via intraperitoneal injection from P2.5 to P9.5. Concentrations were selected based on previous studies (Caballero et al., 2010; Chyu et al., 2004; Frost et al., 2014; Rajeshkumar et al., 2017; Ruan et al., 2019; Stegen et al., 2019). Sodium acetate was dissolved in saline, EGCG, AOA, dimethyl-αKG and GSH-EE were dissolved in DMSO.

Chromatin Immunoprecipitation qRT-PCR (ChIP-qPCR)

ChIP-qPCR was performed as described before (Stegen et al., 2018). Briefly, skeletal progenitor cells and chondrocytes were fixed using 1% formaldehyde, washed and collected by centrifugation (1000xg for 5 minutes at 4°C). The pellet was resuspended in RIPA buffer (50 mM Tris-HCl pH 8, 150 mM NaCl, 2 mM EDTA, 1% Triton-X100, 0.5% sodium deoxycholate, 1% SDS, 1% protease inhibitors), homogenized, incubated on ice for 10 minutes and sonicated. The samples were centrifuged (16000xg for 10 minutes at 4°C) and from the supernatant, shared chromatin was used as input and incubated with an anti-SOX9 (NBP1-85551, Bio-Techne) or anti-H3K27Ac antibody (#8173, Cell Signaling Technology). Rabbit IgG (#2729, Cell Signaling Technology) was used as isotype

control. After precipitation using Pierce Protein A/G Magnetic Beads (Thermo Fisher Scientific), followed by RNA and protein digestion, DNA was purified using Agencourt AMPure XP (Beckman Coulter) according to the manufacturer's instructions. RT-qPCR was performed using SYBR GreenER qPCR SuperMix Universal (Thermo Fisher Scientific) and specific primers for SOX9 binding motifs ((A/T)(A/T)CAA(A/T)G) in the *Gls1* enhancer (#1: Fw 5'-TTGTGTAGGCGCCTTTGT-3', Rev 5'-AATACAGTGGCAGCTCCTTC; #2: Fw 5'-GGCTTGCCAGTAAAGTGAAAC-3', Rev 5'-CCAGAGCTGACCTGATGAAAT-3'; #3: Fw 5'-GGCTTGCCAGTAAAGTGAAAC-3', Rev 5'-CCAGAGCTGACCTGATGAAAT-3'; #4: Fw 5'-CCATGGTGATGCTTAGGTACTG-3', Rev 5'-CTCATCCACAATGGGAG GATTT-3'; #5: Fw 5'-GACTCTCTGGTTCCCAATTCTC-3', Rev 5'-ACTAGTGAGATCCGTTCCTC-3'; #6: Fw 5'-GGAGGAATTGGGA CATGGATAA-3', Rev 5'-TGCACAAACCAAATCTGATTCC-3'; #7: Fw 5'-GCTCAAAGGAAATAAGGCCAGA-3', Rev 5'-CGTGAGCA CATTCACACGTA-3') and *c-Myc* enhancer (#1: Fw 5'-CCGGTGGAGATAATGCTGAA-3', Rev 5'-GCTTCCTGTTCAAATTCCATGT -3'; #2: Fw 5'-TGCTAGCATCCTCATGAATCTT-3', Rev 5'-GACTGAATTGTGTTGGCTCATT-3'; #3: Fw 5'-ACGGGACTCTT GAAGCTTTG-3', Rev 5'-GAGATGTCCCACAGAACAGATG-3'; #4: Fw 5'-GCACGTTTCACACTGAATCTTTAT-3', Rev 5'-ACATCA TACTTCTGAGCCTTGTT-3'; #5: Fw 5'-GGTGTTGAAGTCTCCCACTATT-3', Rev 5'-GCTAAACTCTGAGGAAGCTCTG-3'; #6: Fw 5'-CCAGCCCACACATGACTAAA-3', Rev 5'-GCTTCAGTTCCCTCTTACTGTC-3'; #7: Fw 5'-AAGAGGGAACTGAAGCATAGA-3', Rev 5'-TTCTTCTTCTCCTTCTTATCAATGG-3'; #8: Fw 5'-GGAAGCTAAGGGTATCACACAA-3', Rev 5'-GTGTAGCAGAAACCAGA GACTT-3'), or using primers to detect H3K27Ac enrichment in the enhancer region of *Acan* (Fw 5'-CAAGGTCCCTCACTCTCTCT -3', Rev 5'-GGCTGGCTGACTAGGTTTC-3'), *Ccnd1* (Fw 5'- TGGATGCTGGAGGTAAGAGA-3', Rev 5'-GGGAGGAAGATGTTGGT GATAG-3'), *Col2* (Fw 5'-CTGCTGACGCTGCTCAT-3', Rev 5'-GGGAGGGAGTAGGAGGAAA-3'), *Comp* (Fw 5'- GTCAA TAGGCCTGGGAAGATAC-3', Rev 5'-TGCTGCTGGCTTCCATAG-3'), *Hapln1* (Fw 5'- CAGCCTGCCTCACTAGTTTATC-3', Rev 5'-CACTTCGGAGATCATAGCTTGG-3'), *Matn3* (Fw 5'-ACCAGGTTACCTCTACCTCTT-3', Rev 5'-CCACGACTGTTGCCTTTCTA-3'), *Ndfip2* (Fw 5'-GGAGCGACAGGAAGTGAAG-3', Rev 5'-GCTGGTGGTGATCCATCC-3'), *Runx2* (Fw 5'-TCCCGGCACCTTGAAAC -3', Rev 5'-TTCTCCTCTCGCCCTCTC-3'), *Vegf* (Fw 5'- TTGCTGTCACTGCCGTTT-3', Rev 5'-CCGCAGCAATCCATCCTAAA-3'), *Wwp2* (Fw 5'- GTCAGGTGACCGCGCACG-3', Rev 5'-CGCTCCACTTCCGCCTTC-3') and *Xylt1* (Fw 5'- ACGCTGGTGGTGTG GAA-3', Rev 5'-AGATGGGCAGCCAGGTC-3').

(Immuno)histochemistry and Histomorphometry

Histomorphometric analysis of murine growth plates and ectopic implants was performed on paraffin-embedded sections as previously described (Maes et al., 2012; Stegen et al., 2019). Cartilage matrix proteoglycans were visualized by Safranin O staining. To detect apoptosis, TUNEL staining was performed with an In Situ Cell Death Detection Kit (Roche). Sections were permeabilized for 2 minutes on ice in 0.1% sodium citrate containing 0.1% Triton X-100. TUNEL reaction mixture was applied for 1 hour at 37°C.

For immunohistochemistry, staining conditions were slightly adapted according to the type of antibody used. Generally, paraffin sections were de-waxed, rehydrated, incubated with Antigen Retrieval Solution (Dako) and washed in Tris-buffered saline (TBS). Endogenous peroxidase activity was blocked by immersing the sections in 0.3% H_2O_2 in methanol for 20 minutes. Unspecific antibody binding was blocked by incubation of the sections in 2% BSA-supplemented TBS for 30 minutes. Subsequently, sections were incubated overnight with primary antibody against GLS1 (ab93434, Abcam), Ki67 (proliferating cells; NCL-Ki67p, Leica Biosystems), COL2 (cartilage; MAB8887, Chemicon), H3K9Ac (histone acetylation; #9649, Cell Signaling Technology) or 8OHdG (oxidative DNA damage; ab10802, Abcam). Signal visualization was obtained using fluorophore-labeled secondary antibodies. For COL2 immunostaining, sections were pre-digested with 0.025% pepsin in 0.2 N HCl for 10 minutes at 37°C, fixed in 4% paraformaldehyde, treated with 0.2% Triton X-100 and quenched in 50 mM NH_4Cl prior to incubation with the primary antibody. Sections were counterstained with Hoechst to visualize nuclei. All stainings were quantified on the total growth plate area unless otherwise specified.

Body Composition Analysis

Fat and lean mass were analyzed in 2-week-old male mice using echo resonance scanning (EchoMRI Whole Body Composition Analyzer; EchoMRI LLC, USA) and expressed as percentage of body weight.

RNA and Protein Expression Analysis

RNA Expression

Total RNA from cultured cells, isolated growth plates or ectopic implants was extracted using the NucleoSpin RNA isolation kit (Machery Nagel) and mRNA was reverse transcribed using Superscript II Reverse Transcriptase (Thermo Fisher Scientific). qRT-PCR was performed on the 7500 Fast Real-Time PCR System (Applied Biosystems) using specific forward and reverse oligonucleotide primers (Table S2). Expression levels were analysed using the $2^{-\Delta\Delta Ct}$ method and were normalized for *Hprt* expression.

Protein Expression

Total cell lysates were obtained by lysing cells in 62.5mM Tris buffer (pH 6.8) containing 10% glycerol, 2% SDS, 1x cOmplete protease inhibitor cocktail (Roche) and 1x PhosSTOP phosphatase inhibitor cocktail (Roche). Nuclear protein fractions were prepared by lysing the cells first in a hypotonic buffer (20 mM Hepes pH 7.9, 10 mM KCl, 1.5 mM $MgCl_2$, 1 mM EDTA, 0.5% NP40, 1 mM DTT, supplemented with 1 mM Na_3VO_4, 20 mM NaF, 1 mM PMSF, 5 μg/ml aprotinine, 5 μg/ml leupeptin and 0.33 μg/ml antipain) for 15 minutes at 4°C followed by mechanical disruption of the cell membranes. Nuclei were pelleted from the lysates by centrifugation. The pellet was resuspended in a nuclear extraction buffer (50 mM Hepes pH 7.9, 500 mM NaCl, 1% NP40, supplemented with 1 mM PMSF, 5 μg/ml aprotinine, 5 μg/ml leupeptin and 0.33 μg/ml antipain) and after sonication incubated for 15 minutes at 4°C. Protein concentrations were determined with the BCA Protein Assay Reagent (Thermo Fisher Scientific).

Proteins were separated by SDS-PAGE under reducing conditions and transferred to a nitrocellulose membrane (GE Healthcare). Membranes were blocked with 5% dry milk or BSA in TBS with 0.1% Tween-20 for 30 minutes at room temperature and incubated overnight at 4°C with primary antibodies against AMPK (#2532, Cell Signaling Technology), p-AMPK^{T172} (#2535, Cell Signaling Technology), β-actin (A5441, Sigma-Aldrich), c-MYC (#5605, Cell Signaling Technology), GLS1 (ab93434, Abcam), GLUD1 (ab166618, Abcam), GOT2 (ab171739, Abcam), total H2A (#12349, Cell Signaling Technology), H2AK5Ac (#2576, Cell Signaling Technology), total H3 (#4499, Cell Signaling Technology), H3K4Ac (ab176799, Abcam), H3K9Ac (#9649, Cell Signaling Technology), H3K14Ac (#7627, Cell Signaling Technology), H3K27Ac (#8173, Cell Signaling Technology), H3K9Me2 (ab176882, Abcam), H3K27Me3 (ab192985, Abcam), total H4 (#13919, Cell Signaling Technology), H4K8Ac (#2594, Cell Signaling Technology), or SOX9 (NBP1-85551, Bio-Techne). Signals were detected by enhanced chemiluminescence (PerkinElmer) after incubation with appropriate HRP-conjugated secondary antibodies.

Proliferation was measured by 5'-bromo-2'-deoxyuridine (BrdU) incorporation, added during the last 4 hours of culture, and detected using the Cell Proliferation Biotrack ELISA system (GE Healthcare), and values were normalized to the amount of DNA.

5-hydroxymethylcytosine (5hmC) Dot Blot

Genomic DNA was isolated using the DNeasy Blood & Tissue Kit (QIAGEN) according to the manufacturer's instructions. Isolated DNA was denatured in 0.4 M NaOH with 10 mM EDTA for 10 minutes at 100°C. Samples were incubated on ice, serially diluted and spotted on a BIOTRANS(+) nylon membrane (MP Biomedicals). The blotted membrane was washed in 2x saline-sodium citrate buffer (Sigma-Aldrich), dried at room temperature, and UV cross-linked. Subsequently, the membrane was blocked with 5% dry milk in TBS with 0.1% Tween-20 for 30 minutes at room temperature and incubated overnight at 4°C with a primary anti-5-hydroxymethylcytosine antibody (39769, Active Motif). The signal was detected by enhanced chemiluminescence (PerkinElmer) after incubation with an HRP-conjugated secondary antibody. Loading of spotted DNA was analyzed by staining the membrane with 0.02% methylene blue.

Metabolic Assays

Energy levels

For determination of energy charge and status, cells were harvested in ice cold 0.4 M perchloric acid supplemented with 0.5 mM EDTA. ATP, ADP and AMP were measured using ion-pair reversed phase high-performance liquid chromatography (HPLC) as previously described (Stegen et al., 2016a, 2019, 2016b). Energy charge was calculated as ([ATP] + ½ [ADP]) / ([ATP] + [ADP] + [AMP]).

Mass Spectrometry

For isotopic labelling experiments, cells were incubated for 72 hours with $^{13}C_6$-glucose, $^{13}C_5$-glutamine, 5-^{13}C-glutamine or $^{13}C_4{}^{15}$N-aspartate (Cambridge Isotope Laboratories). Metabolites for subsequent mass spectrometry analysis were prepared by quenching the cells in liquid nitrogen followed by a cold two-phase methanol-water-chloroform extraction (Lorendeau et al., 2017; Stegen et al., 2019, 2016b). Phase separation was achieved by centrifugation at 4°C. The methanol-water phase containing polar metabolites was separated and dried using a vacuum concentrator. Dried metabolite samples were stored at -80°C.

Gas Chromatography-Mass Spectrometric Analysis

Polar metabolites were derivatized and measured as described before (Lorendeau et al., 2017; Stegen et al., 2019). In brief, polar metabolites were derivatized with 20 mg/ml methoxyamine in pyridine for 90 minutes at 37°C and subsequently with *N*-(tert-butyldimethylsilyl)-*N*-methyl-trifluoroacetamide, with 1% tert-butyldimethylchlorosilane for 60 minutes at 60°C. Metabolites were measured with a 7890A GC system (Agilent Technologies) combined with a 5975C Inert MS system (Agilent Technologies). One microliter of sample was injected in splitless mode with an inlet temperature of 270°C onto a DB35MS column. The carrier gas was helium with a flow rate of 1 ml/min. For the measurement of polar metabolites, the GC oven was held at 100°C for 3 minutes and then ramped to 300°C with a gradient of 2.5°C/min. The MS system was operated under electron impact ionization at 70 eV and a mass range of 100–650 atomic mass units (amu) was scanned. Mass distribution vectors were extracted from the raw ion chromatograms using a custom Matlab M-file, which applies consistent integration bounds and baseline correction to each ion. Moreover, we corrected for naturally occurring isotopes. Total contribution of carbon was calculated using the following equation (Buescher et al., 2015):

$$\text{total contribution of carbon} = \frac{\sum_{i=0}^{n} i * m_i}{n * \sum_{i=0}^{n} m_i}$$

where n is the number of C atoms in the metabolite, i represents the different mass isotopomers and m refers to the abundance of a certain mass. Isotope values were corrected for natural abundance using in-house developed software. For metabolite levels, arbitrary units of the metabolites of interest were normalized to an internal standard and protein content.

Liquid Chromatography-Mass Spectrometric Analysis

Polar metabolites were measured as described before (Elia et al., 2017; Stegen et al., 2019). Targeted measurements of polar metabolites, resuspended in 60% acetonitrile, were performed with a 1290 Infinity II HPLC (Agilent Technologies) coupled to a 6470 triple quadrupole mass spectrometer (Agilent Technologies). Samples were injected onto an iHILIC-Fusion(P) column. The solvent,

composed of acetonitrile and ammonium acetate (10 mM, pH 9.3), was used at a flow rate of 0.100 ml/min. Data analysis was performed with the Agilent Mass Hunter software. Metabolite levels were normalized to protein content.

Glutathione Measurement

For measurement of glutathione, samples were extracted in 150 μl 5% trichloroacetic acid, the extract was centrifuged for 10 minutes at 20,000xg. The supernatant was transferred to a vial, 80 μl was injected onto an Acquity UPLC HSS T3 column (2.1x100 mm, particle size 1.8 μm, Waters Corporation) using an Ultimate 3000 UPLC (Thermo Fisher Scientific) in-line connected to a Q-Exactive OrbiTRAP mass spectrometer (Thermo Fisher Scientific). The column was thermostatted at 37°C. A linear gradient was carried out using solvent A (0.05% formic acid) and solvent B (60% methanol, 0.05% formic acid). Briefly, 1% solvent B was maintained for 10 minutes, then increased to 100% B at 12 minutes and kept at 100 % B for 3 minutes. The gradient returned to 1% solvent B at 16 minutes and allowed to re-equilibrate until 21 minutes. The flow rate was kept constant at 250 μl/minute. Elution of reduced glutathione (GSH) and oxidized glutathione (GSSG) was observed at respectively 3 and 6 minutes. The MS operated in selected ion monitoring mode following isotopic envelope of glutathione with m/z 308.09108 to m/z 318.12516. The mass spectrometer was set to positive ion mode, AGC target of $1e^6$ ions and a maximum injection time of 50 ms. The sheath gas flow was set at 35, the auxiliary gas flow rate at 10. The spray voltage was used at 3.00 kV and the capillary was heated at 350°C. Auxiliary gas heater temperature was placed at 300°C.

Glutamine Consumption

Glutamine consumption was determined by measuring glutamine levels in conditioned medium using the Cedex Bio analyser (Roche), following the manufacturer's instructions and values were normalized to the amount of DNA.

Flow Cytometry

Protein Synthesis

Protein synthesis was analysed using the Click-iT® L-homopropargylglycine (HPG) Alexa Fluor® 488 Protein Synthesis Assay Kit (Thermo Fisher Scientific) according to the manufacturer's instructions. Briefly, adherent chondrocytes were incubated with 50 μM Click-iT® HPG overnight in full chondrocyte culture medium. Cells were then fixed with 3.7% formaldehyde for 15 minutes at room temperature, washed and permeabilized with 0.5% Triton X-100 for 20 minutes at room temperature. Subsequently, cells were incubated with Click-iT® reaction cocktail for 30 minutes at room temperature protected from light, washed, trypsinized and fluorescence was detected by flow cytometry. Data were analyzed using Kaluza software (Beckman Coulter) and plotted as mean fluorescence intensity.

Cell Cycle Analysis

Cell cycle analysis was performed using propidium iodide DNA staining. Chondrocytes were trypsinized and fixed in ice-cold 70% ethanol for 1 hour at 4°C. Subsequently, cells were centrifuged, the pellet was incubated with 0.5 mg/ml RNase A and 10 μg/ml PI staining solution and fluorescence was determined by flow cytometry. Data were analyzed using Kaluza software.

Reactive Oxygen Species (ROS) Levels

Intracellular ROS levels were detected by the use of a fluorescent probe dye, CM-H_2DCFDA (Thermo Fisher Scientific). Chondrocytes were incubated with 5 μM CM-H_2DCFDA for 30 minutes at 37°C, and fluorescence was detected by flow cytometry. Data were analyzed using Kaluza software and plotted as mean fluorescence intensity.

Cell Viability

Cell death of cultured chondrocytes or freshly isolated growth plate chondrocytes was detected by flow cytometry using Annexin V-FITC and PI (Dead Cell Apoptosis Kit; Thermo Fisher Scientific) as described before (Stegen et al., 2016b), where Annexin V^- PI^- cells were considered viable. Data were analyzed using Kaluza software.

Collagen Synthesis

Collagen synthesis was quantified *in vitro* by incubation of cultured chondrocytes with 20 uCi/ml ^{3}H-proline (PerkinElmer) as described before (Stegen et al., 2019). After overnight labelling, cells were lysed in extraction buffer (11% acetic acid H_2O with 0.25% BSA) and proteins were precipitated by the addition of 20% trichloroacetic acid. Radioactivity was determined by liquid scintillation counting, and normalized for DNA content.

QUANTIFICATION AND STATISTICAL ANALYSIS

Data are presented as means ± SEM or means ± SD. *n* values represent the number of independent experiments performed or the number of individual mice phenotyped. For each independent *in vitro* experiment, at least three technical replicates were used. For immunoblots, representative images were shown of at least three independent experiments using samples from different cell lysates. Data were analysed by two-sided two-sample Student's t-test, and one-way or two-way ANOVA with Tukey-Kramer post-hoc test using the NCSS statistical software. Differences were considered statistically significant at $p<0.05$.

ADDITIONAL RESOURCES

This study did not generate additional resources.